Atmos. Meas. Tech. Discuss., 8, 9289–9338, 2015
www.atmos-meas-tech-discuss.net/8/9289/2015/
doi:10.5194/amtd-8-9289-2015

Atmospheric Measurement Techniques Discussions

Study of aerosol microphysical properties profiles retrieved from ground-based remote sensing and aircraft in-situ measurements during a Saharan dust event

M. J. Granados-Muñoz[1,2,a], J. A. Bravo-Aranda[1,2], D. Baumgardner[3], J. L. Guerrero-Rascado[1,2], D. Pérez-Ramírez[4,5], F. Navas-Guzmán[6], I. Veselovskii[7], H. Lyamani[1,2], A. Valenzuela[1,2], F. J. Olmo[1,2], G. Titos[1,2], J. Andrey[8,b], A. Chaikovsky[9], O. Dubovik[10], M. Gil-Ojeda[8], and L. Alados-Arboledas[1,2]

[1]Andalusian Institute for Earth System Research (IISTA-CEAMA), Avd. del Mediterráneo, 18006, Granada, Spain
[2]Dpt. Applied Physics, University of Granada, Fuentenueva s/n, 18071, Granada, Spain
[3]Droplet Measurement Technologies, Boulder, CO 80301, USA
[4]Mesoscale Atmospheric Processes Laboratory, NASA Goddard Space Flight Center, 20771, Greenbelt, Maryland, USA

[5]Universities Space Research Association, 21044, Columbia, Maryland, USA
[6]Institute of Applied Physics (IAP), University of Bern, Bern, Switzerland
[7]Physics Instrumentation Center of General Physics Institute, Troitsk, Moscow Region, 142190, Russia
[8]Instituto Nacional de Técnica Aeroespacial (INTA), Ctra. Ajalvir km. 4, 28850 Torrejón de Ardoz, Spain
[9]Institute of Physics, National Academy of Science, Minsk, Belarus
[10]Laboratoire d'Optique Atmospherique, CNRS Universite de Lille 1, Bat P5 Cite scientifique, 59655 Villeneuve d'Ascq CEDEX, France
[a]currently at: Table Mountain Facility, NASA/Jet Propulsion Laboratory, California, Institute of Technology, Wrightwood, California, USA
[b]currently at: CNRM-GAME, Météo-France, Tolouse, France

Received: 18 August 2015 – Accepted: 20 August 2015 – Published: 9 September 2015

Correspondence to: M. J. Granados-Muñoz (mjgranados@ugr.es)

Published by Copernicus Publications on behalf of the European Geosciences Union.

AMTD
8, 9289–9338, 2015

Abstract

In this work we present an analysis of mineral dust optical and microphysical properties obtained from different retrieval techniques applied to active and passive remote sensing measurements, including a comparison with simultaneous in-situ aircraft measurements. Data were collected in a field campaign performed during a mineral dust outbreak a Granada, Spain, experimental site (37.16° N, 3.61° W, 680 m a.s.l.) on the 27 June 2011. Column-integrated properties are provided by sun- and star-photometry which allows a continuous evaluation of the mineral dust optical properties during both day and night-time. Both the Linear Estimation and AERONET (Aerosol Robotic Network) inversion algorithms are applied for the retrieval of the column-integrated microphysical particle properties. In addition, vertically-resolved microphysical properties are obtained from a multi-wavelength Raman lidar system included in EARLINET (European Aerosol Research Lidar Network), by using both LIRIC (Lidar Radiometer Inversion Code) algorithm during daytime and an algorithm applied to the Raman measurements based on the regularization technique during night-time. LIRIC retrievals reveal several dust layers between 3 and 5 km a.s.l. with volume concentrations of the coarse spheroid mode up to 60 $\mu m^3\,cm^{-3}$. The combined use of the regularization and LIRIC methods reveals the night-to-day evolution of the vertical structure of the mineral dust microphysical properties and offers complementary information to that from column-integrated variables retrieved from passive remote sensing. Additionally, lidar depolarization profiles and LIRIC retrieved volume concentration are compared with aircraft in-situ measurements. This study presents for the first time a comparison of both volume concentration and dust particle polarization ratios measured with in-situ and remote sensing techniques. Results for the depolarization measurements in the dust layer indicate reasonable agreement within the estimated uncertainties. The differences in the volume concentration profiles, although somewhat larger, are still within the expected uncertainties.

AMTD
8, 9289–9338, 2015

1 Introduction

Mineral dust is estimated to be the most abundant aerosol type in the atmosphere (∼ half of the total global aerosol burden) (e.g. Textor et al., 2007; Choobari et al., 2014), with global emission between 1000 and 3000 Mt yr^{-1} (Zender et al., 2003, 2004; Shao et al., 2011). Mineral dust directly scatters and absorbs solar and infrared radiation (Miller and Tegen, 1998), and impacts the optical properties of clouds (Ferek et al., 2000; Rosenfeld et al., 2001; Creamen et al., 2013). In addition, mineral dust particles can act as cloud condensation and ice nuclei (Twohy et al., 2009; Ansmann et al., 2009a; DeMott and Prenni, 2010) and affect air quality (Fairlie et al., 2010). The high temporal and spatial variability of dust particles and the complexity in their microphysical and optical properties present a significant challenge to our understanding of how these particles impact the environment.

Numerous field campaigns have been conducted to better characterize mineral dust properties, e.g. the Saharan Mineral Dust Experiments SAMUM-1 and SAMUM-2 (Ansmann et al., 2009b, 2011a and references therein) and the Saharan Aerosol Long-Range TRansport and Aerosol Cloud interaction experiment SALTRACE (http://www.pa.op.dlr.de/saltrace/), among others. However, the information on mineral dust properties is still quite scarce (Formenti et al., 2011), even though many measurements worldwide have been made using different approaches. Satellites are providing global coverage but the retrievals of particle properties are affected by large uncertainties (Levy et al., 2013). Moreover, the interaction of dust particles with solar and terrestrial radiation is complex due to their irregular shapes and variable refractive indices (Mishchenko et al., 1997). Because of this, in the past years it has been difficult to develop accurate algorithms for the retrieval of dust microphysical properties from optical measurements. Dubovik et al. (2006), one of the first studies that addressed this problem, developed an algorithm that took into account the scattering patterns of non-spherical particles and implemented an inversion method for column-integrated radiometric measurements in the AERONET (Aerosol Robotic Network) net-

AMTD
8, 9289–9338, 2015

work (http://aeronet.gsfc.nasa.gov/, Holben et al., 1998). Other approximations using non-spherical particles have also been proposed, e.g. Olmo et al. (2006), Valenzuela et al. (2012a).

Information on the vertical distribution of mineral dust properties is also essential for understanding particle transport processes from regional to intercontinental scales, to improve radiative forcing calculations and to analyze the influence of mineral dust on cloud formation (Ansmann et al., 2008, 2009, 2011a; Seifert et al., 2010). Therefore, it is crucial to develop advanced methods to characterize dust microphysical properties from remote sensors like multi-wavelength Raman lidar or High Spectral Resolution *Lidar* (HSRL) systems (Müller et al., 2010; Veselovskii et al., 2010). In this framework Veselovskii et al. (2010) implemented the kernel functions of Dubovik et al. (2002) in a regularization technique (Müller et al., 1999; Veselovskii et al., 2002) to obtain vertically-resolved dust properties. This approach was first implemented using data of the SAMUM field campaign (Müller et al., 2013) and from measurements of long-range transport of dust over Europe (e.g. Veselovskii et al., 2010; Papayannis et al., 2012).

Raman or HSRL systems have limitations such as the low signal-to-noise ratio, which limits their use mostly during night-time, and the high cost and maintenance. Hence, their implementation is not very widespread. On the contrary, elastic backscatter lidar systems offer an easier set-up and maintenance and larger signal-to-noise ratio during daytime. Their operation is much more extended worldwide due to implementation in networks such as EARLINET (European Aerosol Research Lidar Network) (Pappalardo et al., 2014) and MPLNET (Micro Pulse Lidar Network). In this context, the LIRIC (Lidar Radiometer Inversion Code) code was developed by Chaikovsky et al. (2012) to obtain vertically-resolved profiles of aerosol microphysical properties by combining elastic lidar measurements and column-integrated sun-photometer microphysical properties retrieved from AERONET.

The first results obtained with LIRIC have already been presented by Wagner et al. (2013) and Granados-Muñoz et al. (2014); however, a complete evaluation, using ancillary information such as in-situ vertically-resolved measurements, is still lack-

AMTD
8, 9289–9338, 2015

ing. Generally speaking, there have been very few in-situ measurements to directly compare with those made with remote sensors. Murayama et al. (2003) did a direct comparison between lidar derived and in-situ extinction coefficients during the Aerosol Characterization Experiment – Asia (ACE-Asia) and observed that the in-situ measurements produced larger values that the lidar. Comparisons between volume concentrations measured with in-situ instruments and derived from remote sensors are especially rare. Other than the study of Bravo-Aranda et al. (2014), who compared coarse mode mass derived from airborne spectrometer measurements with mass concentrations derived from lidar and observed that the in-situ measurements were larger than the lidar, there are very few direct comparisons in dust layers between the same parameter measured in-situ and remotely. Most comparisons, such as those reported by Weinzierl et al. (2009, 2011) only do a qualitative comparison whereby the relative magnitudes are compared as a function of the altitude rather than directly comparing the absolute quantities.

The objectives of the present study are to analyze the evolution of the microphysical properties of particles in a mineral dust plume using both LIRIC and a regularization technique applied to multiwavelength-Raman lidar measurements (Veselovskii et al., 2010) and to compare LIRIC profiles of particle volume concentration and depolarization ratios with airborne in-situ measurements.

2 Experimental site and instrumentation

2.1 Experimental site

The data from ground based-instrumentation were acquired at the Andalusian Institute for Earth System Research (IISTA-CEAMA) located in the city of Granada (37.16° N, 3.61° W, 680 m a.s.l.; Lyamani et al., 2010; Titos et al., 2012; Valenzuela et al., 2012b). Granada is a medium-size city in the South-East of Spain located in a natural basin, delimited on the East by mountains with peaks up to 3000 m a.s.l. Air masses affecting

AMTD
8, 9289–9338, 2015

the area arrive mainly from the Atlantic Ocean, Central Europe, the Mediterranean Basin and North-Africa (Valenzuela et al., 2012a; Perez-Ramirez et al., 2012a). The number of mineral dust events at the Granada station originating in North Africa is quite high, especially during summer, with an occurrence of 45 % of the days in June, July and August (Valenzuela et al., 2012b). These events can transport particles at altitudes of up to 5500 m a.s.l., not always affecting the surface level (Guerrero-Rascado et al., 2008, 2009; Navas-Guzmán et al., 2013). The experimental site is also impacted by anthropogenic particles from local and regional aerosol sources (Lyamani et al., 2008, 2010, 2012; Titos et al., 2014).

2.2 Ground-based instrumentation

The Raman-lidar MULHACEN (based on LR331D400, Raymetrics, Greece) used for aerosol vertical-profiling is described in detail by Guerrero-Rascado et al. (2008, 2009) and Navas-Guzmán et al. (2011). It employees a Nd:YAG laser that emits at three different wavelengths (355, 532 and 1064 nm). The receiving system consists of detectors that split the radiation according to the three elastic channels (355, 532 and 1064 nm), two nitrogen Raman channels (387, 607 nm) and a water vapour Raman channel (408 nm). These Raman measurements have sufficient signal-to-noise ratio only for night-time detection. The system also measures depolarization of the returned signal at 532 nm (532-cross and 532-parallel detection channels) (Bravo-Aranda et al., 2013) for retrieving vertical profiles of the particle linear depolarization ratio ($\delta_\lambda^{\mathrm{P}}$). The estimated uncertainties associated with the lidar signals are between ±15 and 20 % for the aerosol particle backscatter coefficient, $\beta_\lambda^{\mathrm{aer}}$, and ± 20 % for the aerosol particle extinction coefficient, $\alpha_\lambda^{\mathrm{aer}}$. These estimates are based on the statistical uncertainties retrieved with Monte Carlo techniques according to Pappalardo et al. (2004) and Guerrero-Rascado et al. (2008). The procedure described by Wandinger and Ansmann et al. (2002) to correct the incomplete overlap of the system is applied to our data. The use of this overlap correction allows to obtain reliable $\beta_\lambda^{\mathrm{aer}}$ profiles at 355 and 532 nm down to 320 m above the station (Navas-Guzmán et al., 2011);

AMTD
8, 9289–9338, 2015

however, reliable data are obtained only from ∼ 1000 m above the station for $\alpha_{\lambda}^{\mathrm{aer}}$. The Raman lidar system is part of EARLINET and currently is included in the ACTRIS (Aerosols, Clouds, and Trace gases Research InfraStructure Network) European project (http://www.actris.net/).

Sun photometric measurements obtained at Granada are used to obtain column-integrated aerosol properties using a CIMEL CE-318. This instrument is included in the AERONET-RIMA network (Iberian Network for Aerosol Measurements, federated to AERONET) (http://www.rima.uva.es/index.php/en/) since 2002 and is calibrated following the AERONET protocols. Details about the CIMEL sun-photometer can be found in Holben et al. (1998), however a brief description is presented here. This instrument makes direct sun measurements at 340, 380, 440, 500, 670, 870, 940 and 1020 nm and sky radiance measurements at 440, 670, 870 and 1020 nm. The direct sun measurements are used to retrieve aerosol optical depth (τ_{λ}) at 340, 380, 440, 500, 675, 870 and 1020 nm. The τ_{λ} uncertainties provided by AERONET are ±0.02 for $\lambda < 400$ nm and ±0.01 for $\lambda > 400$ nm. Additionally, the spectral dependency of the τ_{λ} has been considered through the Ångström exponent, α (440–870), calculated in the range 440–870 nm. Also included in the analysis are aerosol optical depths at 500 nm for fine mode (τ_{fine}) and for coarse mode (τ_{coarse}) as well as the fine mode fraction (η) (ratio of τ_{fine} to τ), determined using the spectral de-convolution algorithm method developed by O'Neill et al. (2003). In addition, column-integrated aerosol microphysical properties (size distribution, refractive index, volume concentration, etc.) provided by the AERONET code are also used (Dubovik and King, 2000; Dubovik et al., 2002, 2006). For the retrieval of the aerosol microphysical properties both the direct sun and the sky radiance measurements are used. The reported size distribution retrieval uncertainties are ±10–35 %, for the size range 0.1 µm $< r <$ 7 µm, and outside this range they are as large as ±80–100 %. All the data used here are Level 1.5 data obtained using the AERONET Version 2 algorithm. Only a small number AERONET Level 2.0 were available due to the restrictions imposed by AERONET code ($\tau_{440\,\mathrm{nm}} > 0.4$ and solar zenith angle > 50°). Therefore, AERONET Level 1.5 (cloud screened data with

AMTD
8, 9289–9338, 2015

pre- and post-calibrations applied) were used in this study, considering only those data that fulfil the following conditions to assure their quality: $\tau_{440\,nm} > 0.2$ and solar zenith angle > 50°.

The star-photometer EXCALIBUR provides τ_λ measurements from the stars' direct irradiance using interferential filters at 380, 436, 500, 670, 880 and 1020 nm (nominal wavelengths) using a CCD camera as detector during night-time. More details can be found in Perez-Ramirez et al. (2008a, b). A regular calibration of the instrument is performed once a year at a high mountain location. Errors in the τ_λ are ±0.02 for $\lambda < 800$ nm and ±0.01 for $\lambda > 800$ nm (Perez-Ramirez et al., 2011). Data are cloud-screened and quality assured over 30 min intervals (Perez-Ramirez et al., 2012b).

2.3 Aircraft in-situ instrumentation

Meteorological and aerosol particle measurements were made with instruments mounted on a CASA C-212-200 research aircraft operated by the Spanish National Institute of Aerospace Technology (INTA). Details on aircraft measurements can be found in Andrey et al. (2014) and Bravo-Aranda et al. (2015). Here we give a short overview of the instruments used for our study: the Cloud and Aerosol Spectrometer with Polarization detection (CAS-POL) and the the Passive Cavity Aerosol Spectrometer (PCASP-100X).

The CAS-POL measures the light scattered by individual particles passing through a focused 658 nm polarized laser beam (Baumgardner et al., 2001). The instrument makes use of 30 channels logarithmically distributed to cover the 0.51–50 µm size range and depolarization ratios are derived from the light back-scattering patterns from individual particles. In this study, CAS-POL measurements are used to obtain both the aerosol volume concentration and the depolarization ratio. A detailed description of the polarization features of the CAS-POL and associated uncertainties are included in the Appendix.

Additionally, the Passive Cavity Aerosol Spectrometer (PCASP-100X) that provides aerosol size distributions in the 0.1–3 µm diameter range in 15 different bins has been

AMTD
8, 9289–9338, 2015

used in order to enhance the size range provided by the CAS-POL measurements. The measuring principle and uncertainties (20 % for the size distributions) have been described in detail by Cai et al. (2013), Rosenberg et al. (2012) and references therein.

3 Methodology: retrievals of aerosol particles microphysical properties

3.1 LIRIC code

The LIRIC algorithm is applied to lidar and sun-photometer data to retrieve aerosol particle microphysical properties profiles during daytime (Chaikovsky et al., 2008, 2012; Wagner et al., 2013; Granados-Muñoz et al., 2014). This algorithm uses as input data the column-integrated optical and microphysical properties retrieved from AERONET code (Dubovik et al., 2002, 2006) and measured lidar elastic backscattered signals at three different wavelengths (355, 532, and 1064 nm). The depolarization information from lidar data can optionally be used. To perform the retrieval, an aerosol model, based on the AERONET code, which assumes a mixture of randomly oriented spheroid and spherical particles defined by the column-integrated volume concentrations of each mode, is used (Dubovik and King, 2000; Dubovik et al., 2006). Subsequently, an iterative procedure based on the Levenberg–Marquardt method is applied. The combined lidar and sun-photometer information provides volume concentration profiles for the fine and coarse modes, distinguishing also between coarse spherical and coarse spheroid particles if depolarization information is considered. The separation between the fine and the coarse modes is made by searching the radius located at the minimum of the AERONET bimodal size distribution in the radii range between 0.194 and 0.576 µm. Uncertainties of the volume concentration profiles related to the different user-defined parameters used within LIRIC algorithm are usually below 15 % (Granados-Muñoz et al., 2014), proving LIRIC to be quite stable. A detailed analysis on the uncertainty due to the input lidar and sun-photometer data uncertainties is still lacking, but it can be estimated for our case. The uncertainty in the retrieved volume

AMTD
8, 9289–9338, 2015

concentration is related to the size distribution that is retrieved from AERONET. As discussed above, this uncertainty can range from 10–35 % if the particle radii are less than 7 µm but can be as much as 100 % if there is significant volume in particles larger than this. As will be illustrated below, measurements of the volume size distribution with the CAS-POL show that there are particles larger than 7 µm radius and in the dust layer they can be larger than 30 µm. Hence, a reasonable estimate of the retrieved volume uncertainty is approximately 50 %, similar to what is estimated for the volume measured by the CAS-POL (see Appendix).

3.2 Inversion of Raman lidar measurements to retrieve microphysical properties

The Raman lidar system provides $\alpha_\lambda^{\mathrm{aer}}$ profiles at 355 and 532 nm, $\beta_\lambda^{\mathrm{aer}}$ at 355, 532, 1064 nm and the $\delta_\lambda^{\mathrm{P}}$ at 532 nm. This $3\beta + 2\alpha + 1\delta$ data set was inverted to retrieve the aerosol particle microphysical properties using the regularization approach, described in detail by Müller et al. (1999) and Veselovskii et al. (2002, 2004).

To account for mineral dust particles non-sphericity the model of randomly oriented spheroids was used, as described in Veselovskii et al. (2010). Following this approach, the particle volume concentration and effective radius were estimated with an uncertainty of about 50 and 25 %, respectively. The real part of the refractive index, m_{r}, was also estimated, with an uncertainty of ±0.05.

3.3 Inversion of τ_λ spectral measurements from sun- and star-photometry measurements

In the present study, we used column-integrated aerosol properties provided by AERONET. These variables were retrieved by inversion of τ_λ and sky radiances using the AERONET operational algorithm. In addition to these AERONET aerosol retrievals, we inverted τ_λ spectral values obtained from both the sun- and the star-photometer with the Linear Estimation (LE) algorithm to get aerosol particle properties (e.g. integrated

AMTD
8, 9289–9338, 2015

volume and effective radius) with high temporal resolution (Kazadzis et al., 2014). The LE algorithm is described in Veselovskii et al. (2012) and more details are provided by Perez-Ramirez et al. (2015), where correction functions to get accurate aerosol data close to that of the operational AERONET code were introduced.

4 Results and discussion

4.1 Overview of the measurement campaign

Different models such as NAAPS (Navy Aerosol Analysis and Prediction System) (Christensen, 1997) and BSC-DREAM8b (Pérez et al., 2006a, b; Basart et al., 2012), forecast mineral dust over the Granada station on the 27 June 2011. Based on these forecasts, a measurement campaign was launched using all the available instrumentation at the IISTA-CEAMA experimental station in coincidence with a simultaneous flight of the CASA C-212-200 research aircraft. The flight took place around 10:30 UTC and the aircraft performed a pseudo spiral track flying from 1200 to 5200 m a.s.l. at a distance of approximately 8 km from the IISTA-CEAMA station. A detailed description of the field campaign and an analysis of the aerosol optical properties retrieved from the ground-based instrumentation are presented by Bravo-Aranda et al. (2015), with a main focus on the analysis of the entrainment and mixing processes of the mineral dust layer within the planetary boundary layer. In our study, however, the main focus is on the evolution of the aerosol optical and microphysical properties evaluated with different instrumentation and different approaches, including a comparison of LIRIC volume concentration and lidar depolarization ratio profiles with in-situ aircraft measurements.

Figure 1 shows the range corrected signal (RCS) time series measured by the lidar on the 27 June 2011. Measurements were performed between 00:00 and 01:00 UTC and 06:45 and 12:10 UTC. According to the lidar measurements, a strong backscattered signal associated with long-range transport of mineral dust (as we will show later on) was observed up to 5 km a.s.l. during both sampling periods.

AMTD
8, 9289–9338, 2015

Figure 2 shows columnar aerosol optical and microphysical properties from the sun- and star-photometry measurements. Figure 2a illustrates the temporal trends in the $\tau_{500\,nm}$, and the corresponding contributions of fine (τ_{fine}) and coarse (τ_{coarse}) modes using the Spectral Deconvolution Algorithm (O'Neill et al., 2001a, b; 2003). The τ_λ-related Ångström exponent (AE($\lambda_1 - \lambda_2$)) computed using the wavelengths between 440 and 870 nm (436 and 880 nm for star-photometry) and the fine mode fraction (η) are shown in Fig. 2b. As can be observed, there was a smooth temporal-evolution of the aerosol properties with small variations. $\tau_{500\,nm}$ time series indicated that the aerosol load slightly varied during the analysed period, with values ranging between 0.27 and 0.37. τ_{coarse} was significantly larger than τ_{fine} during the end of the night and day-time measurements whereas τ_{fine} was almost constant around 0.1 during the study period. The simultaneous increase of $\tau_{500\,nm}$ and τ_{coarse} from midnight suggests an increase of the incoming mineral dust in the atmospheric column. However, during the first hours of the night, the fine mode had a relevant contribution to the total $\tau_{500\,nm}$. The AE ranged between 0.80 at night-time and 0.4 during day-time, suggesting a clear predominance of coarse particles that can be associated with the transport of dust particles. However, the larger values obtained at the beginning of the night period are higher than those acquired from AERONET measurements in the presence of mineral dust (e.g. Dubovik et al., 2002), and thus the contribution of fine particles to the aerosol mixture is also considerable.

The evolution of the effective radius, r_{eff}, and the column volume concentration, V, obtained both by LE and AERONET retrievals during day-time and by LE during night-time for the 27 June 2011 is shown in Fig. 2c and d. Good agreement between AERONET and LE retrievals was obtained during daytime corroborating the good performance of the LE method. In addition, continuity between the star- and sun-photometer measurements was observed, which shows the utility of combining both instruments to perform a continuous monitoring of aerosol properties. As observed in Fig. 2c and d, both r_{eff} and V were slightly lower during the night compared to daytime. The r_{eff} values were around 0.3–0.4 µm during night-time and almost constant around

AMTD
8, 9289–9338, 2015

0.5 µm during daytime. These values suggest a predominance of coarse particles in the atmospheric column. The V values were increasing from 0.15 $\mu m^3\,\mu m^{-2}$ during the night up to 0.25 $\mu m^3\,\mu m^{-2}$ in the early morning and then they decreased again down to 0.1 $\mu m^3\,\mu m^{-2}$ at noon. The changes observed in aerosol properties suggest a mixture of different aerosol types changing from night to day.

During the daytime, a comprehensive analysis of the vertically resolved optical properties retrieved by means of Klett-Fernald (Fernald et al., 1972; Fernald, 1984; Klett, 1981) method was presented by Bravo-Aranda et al. (2015). However, a brief discussion is included here to properly discuss the microphysical properties profiles retrieved with LIRIC during daytime.

Figure 3 shows the analysis of backscattered elastic lidar signals for measurements at daytime on the 27 June retrieved by means of the Klett-Fernald inversion method (Fernald et al., 1972; Fernald, 1984; Klett, 1981) using lidar ratio values between 40 and 48 sr^{-1}. Namely, aerosol particle backscatter profiles at 532 nm, $\beta^{aer}_{532\,nm}$, backscatter related Ångström exponent between 355 and 532 nm, β-AE(355–532 nm), and linear particle depolarization profiles, $\delta^{P}_{532\,nm}$, obtained during day-time from lidar elastic measurements are shown. According to the analysis of these optical properties profiles, two different layers can be distinguished. The first layer is in the height range between 3000 and 5000 m a.s.l. In this layer, the $\beta^{aer}_{532\,nm}$ values are decreasing during the morning. For this height range, β-AE(355–532 nm) profiles suggest the predominance of coarse particles with values close to zero during the analysed period, in coincidence with $\delta^{P}_{532\,nm}$ values ($\delta^{P}_{532\,nm}$ in the range 0.23–0.28) that suggest an important contribution of non-spherical particles (Gross et al., 2011). However, below 2000 m a.s.l., β-AE(355–532 nm) was decreasing from 2 in the early morning down to $\sim$ 0.5 around midday. At the same time, $\delta^{P}_{532\,nm}$ was increasing from 0.08 up to 0.20. During the morning, these results suggest the influence of anthropogenic particles from local origin that is mixed with the mineral dust due to convective processes within the planetary mixing layer (Bravo-Aranda et al., 2015).

AMTD
8, 9289–9338, 2015

LIRIC retrievals obtained for the morning of the 27 June 2011 are shown in Fig. 4. A clear predominance of the coarse spheroid mode is observed from the surface up to 5000 m a.s.l., as expected for mineral dust events. In addition, a decrease of the total volume concentration values was observed throughout the morning, in agreement with the decrease in $\beta^{aer}_{532\,nm}$ (Fig. 3) and the decrease in the integrated volume concentration V (Fig. 2d). A maximum peak in the volume concentration of the coarse spheroid mode was observed between 4000 and 4500 m a.s.l., in coincidence with the maximum in $\beta^{aer}_{532\,nm}$ profiles, indicating the presence of an aerosol layer at this height. It is worth noting that fine particles were also observed during the different analysis periods as indicated by the volume concentration profiles, but in low concentrations ($\sim 6\,\mu m^3\,cm^{-3}$). The fact that the profiles of the fine mode volume concentration show a maximum peak at the same height as the coarse spheroid mode suggests that these fine particles could have been advected with the mineral dust. Therefore, they might correspond to the fine mode of mineral dust. There is also the possibility that they correspond to anthropogenic aerosol originating from the industrial areas in the North of Africa together with the mineral dust (Rodríguez et al., 2011; Valenzuela et al., 2012c), as indicated by the backward trajectories analysis performed with HYSPLIT model using GDAS meteorological database (http://ready.arl.noaa.gov/HYSPLIT_traj.php, figure not shown). Another possible explanation is that it could be an artifact introduced by LIRIC due to problems with the incomplete overlap or in cases of non-homogeneous layering (Granados-Muñoz et al., 2014), distributing the contribution of local pollution at high altitudes.

The coarse spherical mode volume concentration slightly increased during the morning reaching its maximum values ($\sim 7\,\mu m^3\,cm^{-3}$) between 11:15 and 11:45 UTC. This slight increase in the volume concentration of the coarse spherical mode (from 0 up to $5\,\mu m^3\,cm^{-3}$) around 4500 m a.s.l. was in agreement with a slight decrease in $\delta^{P}_{532\,nm}$ values (from 0.28 to 0.23) in the same height range, indicating a larger contribution of spherical particles and corroborating once again the coherence between the aerosol optical and microphysical properties profiles obtained.

AMTD
8, 9289–9338, 2015

The layering observed in the optical properties profiles (Fig. 3) indicated the presence of mineral dust in the upper layer between 3000 and 5000 m a.s.l. and the presence of anthropogenic particles in the lower part of the troposphere that was not detected by LIRIC. This can be explained by the fact that LIRIC assumes several AERONET retrieved properties (i. e., refractive index, size distribution, sphericity, etc.) as height-independent and therefore LIRIC results are much more vertically homogeneous regarding the distribution of the modes than those retrieved from the lidar data with Klett-Fernald algorithm. A combined inversion of lidar and sun-photometer data without such assumptions, as the one proposed in GARRLIC (Generalized Aerosol Retrieval from Radiometer and Lidar Combined data) (Lopatin et al., 2013), might provide more accurate results regarding the vertical distribution of the aerosol properties, although GARRLIC is out of the scope of this work. Meanwhile, the interpretation and analysis of the LIRIC-retrieved volume concentration profiles needs to be carefully made when the atmospheric aerosol layers comprise different aerosol types, as shown in Granados-Muñoz et al. (2014).

4.2 Night-time retrieval of mineral dust microphysical properties profiles

The Raman $3\beta + 2\alpha + \delta$ measurements on the night previous to the flight were inverted to retrieve vertical profiles of volume concentration, r_{eff} and the real part of the refractive index using the regularization approach (Veselovskii et al., 2010). The comparison of these profiles with LIRIC results using the first data of the day, acquired at 06:15–06:45 UTC, allow us to see the evolution of the vertical structure of the aerosol microphysical properties. A comparison of both techniques over the same time period was not possible due to the lack of simultaneous data.

Figure 5a and b show the optical properties retrieved with the Raman method during night-time (averaged between 00:00 and 01:00 UTC). The optical properties shown in Fig. 5a and b indicate values of $\beta^{\text{aer}}_{532\,\text{nm}}$ similar to those observed in Fig. 3, corresponding to the period between 06:15 and 06:45 UTC. However, the vertical structure of the aerosol layer was different, corroborating the evolution of the aerosol vertical struc-

AMTD
8, 9289–9338, 2015

ture during the night. As can be observed, two peaks were detected during night-time around 3200 and 4200 m a.s.l. whereas a much more homogeneous structure was observed during daytime, with only one maximum at 4100 m a.s.l. The $\delta^{P}_{532\,nm}$ profiles and its inverse correlation with β-AE(355–532 nm) in Fig. 5b corroborates also the presence of two differentiated regions with different aerosol types during night-time, namely there were mineral dust particles above 2250 m a.s.l. ($\delta^{P}_{532\,nm} \sim 0.25$) and a mixing of local anthropogenic aerosol with mineral dust below this height. Values of the different aerosol properties in both regions are shown in Table 1.

The overlap effects prevented using extinction data below 2000 m and therefore inversion of microphysical properties was not possible below this height. For the inversion, the optical data were averaged in 250 m layers for the heights between 2000 and 3600 m a.s.l. Above that height averaging was done in 1000 m layers. Figure 5c–e shows the corresponding microphysical properties obtained by the regularization technique. As we can observe in Fig. 5c, r_{eff} values varied in the different layers. The highest values, $\sim$ 1.76 µm, related to larger particles (mineral dust), were found in the layer between 2500 and 3500 m a.s.l., while the smallest values, $\sim$ 0.53 µm, were found in the lower layer. Values around 4200 m a.s.l. ($\sim$ 1.1 µm) are still larger than those in the lower layer, but lower than in the maximum around 3200 m a.s.l. This decrease in the radius with height can be due to an artifact of the algorithm because of the larger averaging height interval used in the upper part of the profiles and not necessarily related to a decrease in the size of the particles. Volume concentration values were also larger for the dust layer than for the one with mixed particles. This fact can be explained by both the volume concentration dependence on particle radius and also the larger aerosol load in this layer (as observed in the layering structure of $\beta^{aer}_{532\,nm}$ in Fig. 5a). Two regions were also clearly distinguished in the m_r profile obtained with the regularization technique. The m_r values were larger in the upper part of the profile, corresponding to the mineral dust layer and lower values were obtained in the lower part of the profile, due to the presence of the mixture of mineral dust and anthropogenic particles. The mean value of m_r in the profile was 1.55 ± 0.05. Figure 5e shows the volume size dis-

AMTD
8, 9289–9338, 2015

tributions for different altitudes. The volume size distribution at the surface level was obtained from the Aerodynamic Particle Sizer (APS-3321, TSI) (Volcken and Peters, 2003; Lyamani et al., 2010). The APS is an aerosol optical counter that measures aerosol particle size distribution and concentration in the aerodynamic radius range between 0.25 and 10 µm in 52 nominal size bins. Therefore most of the fine mode is not detected. The volume size distributions at higher altitudes were obtained by the regularization technique. In addition, the closer in time column-integrated AERONET size distribution (26 June 2011 at 18:15 UTC) was included. From both APS and lidar measurements, it was observed a clear increase in the coarse mode radius with height, as the location of the maximum is displaced towards larger radii, in agreement with r_{eff} profiles. There was also an increase of the aerosol load since the maximum in the volume concentration strongly increased with height. Fine mode was almost insignificant in the different layers. However, the AERONET column-integrated distribution showed a small contribution of the fine mode aerosol particles and also the coarse mode radius shifted to smaller values. This can be explained by the presence of mineral dust particles at higher altitudes while at lower levels dust was mixed with local anthropogenic pollution. In the first 400 m above ground it seemed that fine aerosol particles predominated, but because of the lidar incomplete overlap and the limitations of the APS this could not be confirmed. However, in-situ measurements presented by Bravo-Aranda et al. (2015) pointed in this direction.

4.3 Comparison of airborne in-situ measurements and ground-based retrieved profiles

Figure 6a shows the vertical profiles of the volume concentration derived from the AERONET and lidar measurements using the LIRIC algorithm and from the aircraft in-situ measurements. Since AERONET size distribution includes only particles up to 10 µm radius, in order to make a coherent comparison only particles below 20 µm diameter measured by the CAS-POL were considered in the calculations of the volume concentration profile (red profile in Fig. 6a). A second profile including the complete size

AMTD
8, 9289–9338, 2015

distribution from the CAS-POL (black profile in Fig. 6a) is also included for completeness. For the retrieval of the volume concentration profiles from the in-situ aircraft measurements, a refractive index of 1.54 (real part) (McConnell et al., 2010) was assumed and Mie theory was applied assuming spherical aerosol particles as explained by Andrey et al. (2014). This refractive index value is very similar to the one obtained with the regularization technique for the night-time measurements, which was 1.55 ± 0.05. The agreement in the vertical structure between the aircraft and LIRIC volume concentration profiles was quite good with respect to the location of the peaks. Similar layering was detected with both LIRIC and the airborne data, distinguishing two maximum peaks around 3500 and 4200 km a.s.l. The height of the first maximum obtained by aircraft in-situ measurements was located at a slightly higher altitude (3450 m a.s.l.) than by the LIRIC algorithm (3250 m a.s.l.). The geometrical thickness of the different layers observed were also very similar for both LIRIC and the aircraft data.

Regarding the volume concentration values, the differences are within the expected uncertainties, marked by the horizontal bars in Fig. 6. In general, average in-situ values exceed those from LIRIC by less than 20 $\mu m^3 cm^{-3}$, except for the concentration maximum between 3200 and 3500 m if we consider only particles below 10 µm. Differences are much larger if we compare LIRIC retrieval to the volume concentration profiles retrieved using the complete size distribution provided by the CAS-POL. The difference between the two profiles retrieved from the aircraft in-situ measurements reveals a likely underestimation of the volume concentration profiles retrieved by LIRIC by some fraction that depends on the amount of particle volume in sizes larger than 10 µm (in radius) not considered in AERONET. A similar behaviour was found by Bravo-Aranda et al. (2014): when comparing the dust mass concentration retrieved by applying the POLIPHON (Polarizing Lidar Photometer Networking) method to lidar data (Ansmann et al., 2011b) with the coarse-mode mass concentration derived from the aircraft measurements (assuming a density of 2.6 $g cm^{-3}$ for the mineral dust) larger differences where observed in the maximum peaks and a similar displacement of the aerosol layers was found. The difference between the in-situ and remote sensing concentrations

AMTD
8, 9289–9338, 2015

raises the question as to which technique is providing the more accurate value. Both techniques rely on certain assumptions that could potentially bias the results. In the discussion of the CAS-POL uncertainties in the Appendix, the two most important assumptions are related to the refractive index and shape of the particles. If the refractive index of the particles differ from what is assumed, this can bias the sizing either smaller or larger, but no more than 50 %. The assumption that the particles are spherical will bias the sizes, and hence the volumes, perhaps even as much as a factor of two if the dust particles are very aspherical. This could explain the discrepancies between the two techniques over most of the profiles where the differences are within a factor of two. Countering that argument, however, is the comparison of the size distributions measured with the combined PCASP-100X and the CAS-POL and those derived from AERONET. Figure 7 shows average size distributions in the five altitude ranges labelled (1) through (5) in Fig. 6a. When compared with the size distributions derived from AERONET (Fig. 5d), we observe that both measurements show a very similar distribution (note that AERONET reports in radius whereas the CAS-POL measurements are in EOD), e.g. the peak volume falls at 10 µm EOD (5 µm radius). This suggests that the larger volume reported from the CAS-POL is not a result of oversizing.

In situ measurements of depolarization ratios from aircraft have never been published before so the results presented here are the first opportunity to compare profiles from aircraft with those derived from remote sensors. The CAS-POL mean depolarization ratio at a wavelength of 680 nm is compared with the $\delta^{\mathrm{P}}_{532\,\mathrm{nm}}$ profile retrieved at 10:30 UTC from the lidar data (Fig. 6b). The uncertainty of the depolarization ratio from the CAS-POL measurements is estimated to be around 30 % (see Appendix), similar to what is estimated for the lidar. The horizontal bars on each curve illustrate these uncertainties. In general, we observe reasonable agreement in the trends derived from lidar $\delta^{\mathrm{P}}_{532\,\mathrm{nm}}$ profiles and CAS-POL, especially in the layer between 4000 and 4500 m a.s.l., where discrepancies are close to 0. In the rest of the profile, the CAS-POL values are somewhat larger than the lidar-retrieved $\delta^{\mathrm{P}}_{532\,\mathrm{nm}}$. Nonetheless, the discrepancies are below 15 % for most part of the profile, which is within the uncertainty limits, corrobo-

AMTD
8, 9289–9338, 2015

rating the good performance of both techniques. It is worth noting that not only does the CAS-POL measure the scattered light at a longer wavelength than the lidar, but in addition, whereas the lidar measures at 180° backscatter, the CAS-POL is measuring over backscattering angle from 168 to 176°. The importance of this difference can be seen in Fig. 8 that shows theoretical calculations of polarization ratio as a function of scattering angle and different shapes (courtesy of P. Yang, Texas A&M University). The shapes are those of different types of ice crystals but serve equally well to demonstrate the degree of depolarization as a function of the measurement angle. The polarization ratio defined here are from Stokes matrix components P_{11} and P_{22}. For linearly polarized incident light, the ratio of P_{22}/P_{11} is the inverse of what is reported from the lidar and CAS-POL. What is important to note is that for all of the shapes except rough aggregates, the ratio is smaller at 180° than for the 168 to 176° range. Rough aggregates are quasi-spherical whereas dust is likely more aspherical leading to the observation that the higher polarization ratios measured by the CAS-POL may be mostly due to the difference in collection angles.

5 Summary and conclusions

An exhaustive measurement campaign was performed on the 27 June 2011 at Granada station during a Saharan dust outbreak. Active and passive remote sensing techniques were used to continuously monitor the atmosphere together with in-situ measurements on board an aircraft. This study focused particularly on the analysis of the microphysical properties, column integrated and vertically resolved, implementing different processing algorithms, i.e. LIRIC, the regularization method and the Linear Estimation technique. To our knowledge this is the first time that these techniques are processed and compared together along with a direct comparison between in-situ aircraft and remote sensing measurements.

Column-integrated properties were retrieved by means of star and sun-photometer measurements. Night-to-day evolution of the aerosol optical depth at 500 nm and the

AMTD
8, 9289–9338, 2015

Ångström exponent followed a smooth behaviour explained by the natural variability of the aerosol particle population. The aerosol optical depth at 500 nm ranged between 0.27 and 0.37 during the analysis period, while the Ångström exponent varied from 0.80 at night-time to 0.4 during the day-time. Column-integrated microphysical properties retrieved with the operational AERONET and Linear Estimation codes were in good agreement. Moreover, the Linear Estimation allowed analysis of the temporal-evolution from night- to day-time of effective radius and volume concentration. A smooth temporal-evolution has been observed, with the effective radius ranging between 0.3 and 0.5 µm. The derived Ångström exponent and effective radius suggest a predominance of coarse particles but with some contribution by the fine mode particles, which was significant during some periods.

The analysis of the aerosol optical properties profiles highlighted the presence of two aerosol layers during daytime: a lower layer corresponding to a mixture of anthropogenic aerosol with mineral dust and a higher layer corresponding to pure mineral dust. As expected in presence of mineral dust, the LIRIC analysis indicates a clear predominance of the coarse spheroid mode, with average volume concentrations around 30 $\mu m^3 cm^{-3}$, reaching 60 $\mu m^3 cm^{-3}$ at the maximum peaks. Fine particles were observed in lower concentrations ($\sim 6\ \mu m^3 cm^{-3}$) at high altitudes, suggesting that they could be anthropogenic particles originated in the industrial areas in the North of Africa or they might correspond to the mineral dust fine mode. However, they could also be related to a LIRIC artifact that distributes the local anthropogenic aerosol at higher altitudes. Results obtained with LIRIC are in agreement with the results obtained from the analysis of the optical properties retrieved from the lidar data in the upper layer corresponding to mineral dust. However, there is some disagreement in the lowermost part of the profiles, below 2000 m a.s.l., which corresponds to the mixture of mineral dust with anthropogenic aerosol. These discrepancies are mainly related to the assumption of height-independent aerosol properties in LIRIC and indicate that LIRIC profiles need to be carefully interpreted in cases of non-homogeneous aerosol layers.

AMTD
8, 9289–9338, 2015

The regularization technique applied to the Raman lidar data during the night previous to the flight was used to evaluate the temporal evolution of the aerosol microphysical properties profiles. According to the lidar data, the aerosol backscatter coefficient profiles, β^{aer}_{532nm}, showed larger values during the night than in the early morning in certain layers indicating changes in the aerosol vertical structure due to the temporal evolution of the dust event during the night. The retrievals of total volume concentration profiles at night (with the regularization technique) and in the early morning (with LIRIC) also indicated a decrease in the volume concentration from maximum values of 75–50 $\mu m^3\,cm^{-3}$ and changes in the aerosol vertical structure. However, column integrated values showed small changes in the aerosol properties, remaining almost constant during the night. These results underscore the need for vertically resolved measurements to adequately monitor the evolution of the aerosol properties. The discrepancies between regularization and LIRIC results are mainly explained by the natural variability of the aerosol during the night. Because of this temporal variability, results obtained from the two different approaches are not comparable in absolute terms. However, from our analysis we can conclude that the combined use of LIRIC and the regularization technique improves our capability for evaluating the evolution of microphysical properties profiles during night- and day-time.

For a direct intercomparison of LIRIC with the regularization technique more simultaneous datasets are required. Advances in vibrational Raman will allow measurement of the extinction coefficients during the daytime and measurements from HSRL systems could also help in this aspect. On the other hand, advances in techniques to retrieve microphysical properties from star-photometry will allow the use of LIRIC during night. Improvements in the application of the Linear Estimation method also could be addressed in this way. Such approaches are essential both to study the temporal evolution of aerosol microphysical profiles and also to define strategies for evaluating satellite products.

Profiles of linear particle depolarization retrieved with the lidar data and volume concentration retrieved with LIRIC were compared with CASA C-212-200 aircraft measure-

AMTD
8, 9289–9338, 2015

ments. This study represents the first time that in-situ measurements of particle depolarization ratio have been compared with lidar measurements. The CAS-POL measurements were compared with linear particle depolarization retrieved with the lidar data. The two separate techniques produces results that were within the estimated uncertainties over the whole vertical extent of the measurements. Similarly, the vertical profiles of the volume concentration, retrieved from the combined PCASP-100X and CAS-POL size distributions and LIRIC retrievals were very similar in general shape, i.e. maxima at 3200–3500 and 4100–4400 m were identified by both techniques. The average values were within the estimated uncertainties with discrepancies generally below 20 $\mu m^3 cm^{-3}$ when the same size range was considered for both techniques. The volume concentrations from the CAS-POL are likely overestimates due to the asphericity of the dust particles but the LIRIC derived values are underestimates because of the presence of particles with equivalent optical diameters larger than 20 µm.

The synergy of instruments and different techniques presented in this study reveals the potential to obtain a complete characterization of the aerosol properties using a combination of the measurements. However, future efforts should aim to reduce the uncertainty of the measured and retrieved aerosol properties in order to obtain more reliable and accurate aerosol properties databases.

Appendix: CAS-POL measurement principles and uncertainties

The CAS-POL measures the light that is scattered by individual particles that pass through a focused, 658 nm, polarized laser beam (Baumgardner et al., 2001). Optical components are positioned to collect some of the light that is scattered into a forward cone from 4–12° and a backward cone from 168–176°. The backward scattered light is divided into two components: one that is measured with a detector that is behind an optical filter that passes only the scattered light with polarization that is perpendicular to the polarization of the incident light and another detector with no filter (Glen and Brooks, 2013). The equivalent optical diameter (EOD) of each particle in the nominal

AMTD
8, 9289–9338, 2015

size range from 0.6–50 µm is derived from the peak intensity of the collected forward scattered light using Mie theory (Mie, 1908) and an assumption of particle sphericity at a known refractive index. The terminology, EOD, is used here to underscore that ambient aerosol particles are only spherical if they are liquid or have a liquid coating and the refractive index can vary over a wide range. Hence, the EOD refers to the size of a spherical particle with known refractive index that would have scattered the equivalent intensity of light.

The three signals, forward scattering (FS), backward scattering (BS) and polarized (POL) provide three pieces of information that, from a relative perspective, can differentiate regions of air masses that have different particle characteristics. Although there are currently studies underway that will provide for a more quantitative interpretation of this, for the analysis used in the current study the metrics derived from these signals will be used to compare particle properties in the boundary layer and the free troposphere with and without a dust layer.

The interaction of the linearly polarized laser radiation with a particle leads to scattered light with some of the polarization in the same plane as the incident light and some fraction at a perpendicular plane (Nicolet et al., 2007, 2010, 2012; Schnaiter et al., 2012; Baumgardner et al., 2014). In laboratory studies, Glen and Brooks (2013) showed that the relationships between the FS, BS and POL signals were related to the type of dust, i.e. hematite, quartz and zeolite could be clearly differentiated by comparing the three signals. In the analysis of CAS-POL measurements in the current study, we will only report the depolarization ratio (defined below).

The measurement uncertainties are associated with the accuracy of determining the sample volume and the derivation of the EOD. The estimated uncertainty in the sample volume is ±20 % primarily due to the optical technique used to qualify particles within the beam (Baumgardner et al., 2001). The sizing uncertainty ranges from 20–50 % and depends on the variation in the refractive index and the asphericity of the particles. Figure 9a shows the theoretical scattering cross section (Mie, 1908) of spherical particles as a function of diameter for three refractive indices and the collection angles

AMTD
8, 9289–9338, 2015

of the CAS-POL. Only a small size range is shown in order to illustrate the potential magnitude of uncertainty. The dashed lines show that particles with four different sizes have the same scattering cross section. The scattering intensity is directly proportional to the particle optical cross section; hence, when we measure scattering of this magnitude with the instrument, we do not know if the particle was a water droplet with 1.25, 2.0 or 2.5 µm EOD, a salt particle (NaCl) with a 1.75 or 2.5 µm EOD or a sulfate particle (refractive index of 1.44) with an EOD of 2.5 µm.

The average uncertainty due to deriving an EOD of unknown refractive index was estimated by analyzing the variation in size when assuming a particle had a refractive index of 1.48 then finding what particle size would have the same scattering cross section if it actually had a different refractive index. The calculation was carried out over a range of refractive indices from 1.33 (water) to 1.60 (some types of organics). Figure 9b presents the results of this evaluation where the ordinate is the average derived value for the given size at a refractive index of 1.48 and the vertical bars are one standard deviation around the mean. The red lines are the one-to-one (solid) and ±20 % (dashed) around the one to one. From this figure we see that the uncertainty falls within ±20 % of the assumed values except for the EOD between 2 and 4 µm. Hence, the uncertainty due to the refractive index variations is on average ±20 %.

The uncertainties that are related to the asphericity of a particle are more difficult to estimate since they are dependent on the complexity of the morphology, the degree of asphericity and the orientation of the particle when it passes through the beam. Borrmann et al. (2000) applied **T** matrix theory to estimate the amount of undersizing of prolate and oblate spheroids dependent on their aspect ratios. The change in polarization caused by a particle is also dependent on aspect ratio and orientation. Baumgardner et al. (2014) ran simulations using **T** matrix theory to calculate the depolarization ratio as a function of aspect ratio, size and orientation. The depolarization ratio is defined here as the signal from the polarization detector divided by intensity of scattered light measured by the total backscatter detector (Glen and Brooks, 2013). The variation in the shape and orientation of the particle in the beam leads to uncer-

AMTD
8, 9289–9338, 2015

tainties of the depolarization ratio around 30 %, depending on the aspect ratio of the dust. Figure 10 illustrates the response of the CAS-POL to a 2 µm particle with aspect ratio of 0.9 as a function of its orientation in the beam (alpha and beta designate the angles with respect to the incident laser beam). From this figure we observe that the depolarization ratio can vary from almost zero to more than 0.15, depending on how it is oriented. With no other information available to determine a particle's asphericity, the estimated sizing uncertainty due to the assumption of sphericity is of the order of 50 %.

The errors in the sample volume and size are propagated using the root sum squared (RSS) approach to estimate the uncertainty in the derived bulk parameters of number and volume concentrations and the median volume diameter. These estimated uncertainties are ±20, ±90 and ±50 %, respectively.

Acknowledgements. This work was supported by the Andalusia Regional Government through projects P12-RNM-2409 and P10-RNM-6299, by the Spanish Ministry of Science and Technology through projects CGL2010–18 782, and CGL2013-45410-R; by the EU through ACTRIS project (EU INFRA-2010-1.1.16-262254); and by the University of Granada through the contract "Plan Propio. Programa 9. Convocatoria 2013". CIMEL Calibration was performed at the AERONET-EUROPE calibration center, supported by ACTRIS (European Union Seventh Framework Program, (FP7/2007–2013) under grant agreement no. 262254). Granados-Muñoz was funded under grant AP2009-0552. The authors thankfully acknowledge the computer resources, technical expertise, and assistance provided by the Barcelona Supercomputing Center for the BSC-DREAM8b model dust data. The authors express gratitude to the NOAA Air Resources Laboratory for the HYSPLIT transport and dispersion model and those at the NRL-Monterey that helped in the development of the NAAPS model. We also express our gratitude to the developers of LIRIC algorithm and software. We also thank N. T. O'Neill for providing the Spectral Deconvolution Algorithm used in the star-photometer. Thanks are also due to INTA Aerial Platforms, a branch of the Spanish ICTS program, and the Spanish Air Force for their efforts in maintaining and operating the aircraft. We would like to thank Ping Yang of Texas A&M University for providing the results of his simulations of light scattering from different types of ice crystals.

AMTD
8, 9289–9338, 2015

References

Alados-Arboledas, L., Lyamani, H., and Olmo, F. J.: Aerosol size properties at Armilla, Granada (Spain), Q. J. Roy. Meteor. Soc., 129, 1395–1413, 2003.

Alados-Arboledas, L., Alcántara, A. Olmo, F. J., Martínez-Lozano, J. A., Estellés, V., Cachorro, V., Silva, A. M., Horvath, H., Gangl, M., and Díaz, A.: Aerosol columnar properties retrieved from CIMEL radiometers during VELETA 2002, Atmos. Environ., 42, 2654–2667, 2008.

Andreae, M.: Biomass burning – its history, use, and distribution and its impact on environmental quality and global climate, global biomass burning – atmospheric, climatic, and biospheric implications (A 92-37626 15–42), MA, MIT Press, Cambridge, 3–21, 1991.

Andrey, F. J.: Impacto de las nubes de polvo sahariano sobre las medidas de la columna de ozono desde fotómetros orbitales orientados al nadir, PhD Dissertation, Universidad Autonoma de Madrid, Spain, 2011.

Andrey, J., Cuevas, E., Parrondo, M. C., Alonso-Pérez, S., Redondas, A., and Gil-Ojeda, M.: Quantification of ozone reductions within the Saharan air layer through a 13 year climatologic analysis of ozone profiles, Atmos. Environ., 84, 28–34, 2014.

Ansmann, A., Riebesell, M, and Weitkamp, C.: Measurement of atmospheric aerosol extinction profiles with a Raman lidar, Opt. Lett., 15, 746–748, 1990.

Ansmann, A., Bösenberg, J., Chaikovsky, A., Comerón, A., Eckhardt, S., Eixmann, R., Freudenthaler, V., Ginous, P., Komguem, L., Linne, H., Lopez-Marquez, M. A., Matthias, V., Mattis, I., Mitev, V., Müller, D., Music, S., Nickovic, S., Pelon, J., Sauvage, L., Sobolewsky, P., Srivastava, M., Stohl, A., Torres, O., Vaughan, G., Wandinger., U., and Wiegner, M.: Long-range transport of Saharan dust to northern Europe: the 11–16 October 2001 outbreak observed with EARLINET, J. Geophys. Res.-Atmos., 108, 2156–2202, 2003.

Ansmann, A., Tesche, M., Althausen, D., Müller, D., Seifert, P., Freudenthaler, V., Heese, B., Wiegner, M., Pisani, G., and Knippertz, P.: Influence of Saharan dust on cloud glaciation in southern Morocco during the Saharan mineral dust experiment, J. Geophys. Res.-Atmos., 113, 2156–2202, 2008.

Ansmann, A., Tesche, M., Knippertz, P., Bierwirth, E., Althausen, D., Müller, D., and Schulz, O.: Vertical profiling of convective dust plumes in southern Morocco during SAMUM, Tellus B, 61, 340–353, 2009a.

AMTD
8, 9289–9338, 2015

Ansmann, A., Tesche, M., Seifert, P., Althausen, D., Engelmann, R., Fruntke, J., Wandinger, U., Mattis, I., and Müller, D.: Evolution of the ice phase in tropical altocumulus: SAMUM lidar observations over Cape Verde, J. Geophys. Res.-Atmos., 114, 2156–2202, 2009b.

Ansmann, A., Petzold, A., Kandler, K., Tegen, I., Wendisch, M., Mueller, D., Weinzierl, B., Mueller, T., and Heintzenberg, J.: Saharan mineral dust experiments SAMUM–1 and SAMUM–2: what have we learned?, Tellus B, 63, 403–429, 2011a.

Ansmann, A., Tesche, M., Seifert, P., Groß, S., Freudenthaler, V., Apituley, A., Wilson, M. K., Serikov, I., Linne, H., Heinold, B., Hiebsch, A., Schnell, F., Schmidt, J., Mattis, I., Wandinger, U., and Wiegner, M.: Ash and fine-mode particle mass profiles from EARLINET-AERONET observations over central Europe after the eruptions of the Eyjafjallajökull volcano in 2010, J. Geophys. Res.-Atmos., 116, D00U02, doi:10.1029/2010JD015567, 2011b.

Balis, D. S., Amiridis, V., Nickovic, S., Papayannis, A., and Zerefos, C.: Optical properties of Saharan dust layers as detected by a Raman lidar at Thessaloniki, Greece, Geophys. Res. Lett., 31, L13104, doi:10.1029/2004GL019881, 2004.

Baumgardner, D., Jonsson, H., Dawson, W., O'Connor, D., and Newton, R.: The cloud, aerosol and precipitation spectrometer (CAPS): a new instrument for cloud investigations, Atmos. Res., 59–60, 251–264, 2001.

Baumgardner, D., Newton, R., Krämer, M., Meyer, J., Beyer, A., Wendisch, M., Vochezer, P.: The cloud particle spectrometer with polarization detection (CPSPD): a next generation open-path cloud probe for distinguishing liquid cloud droplets from ice crystals, Atmos. Res., 142, 2–14, 2014.

Bravo-Aranda, J. A., Navas-Guzmán, F., Guerrero-Rascado, J. L., Pérez-Ramírez, D., Granados-Muñoz, M. J., and Alados-Arboledas, L.: Analysis of lidar depolarization calibration procedure and application to the atmospheric aerosol characterization, Int. J. Remote Sens., 34, 3543–3560, 2013.

Bravo-Aranda, J. A., Titos, G., Granados-Muñoz, M. J., Guerrero-Rascado, J. L., Navas-Guzmán, F., Valenzuela, A., Lyamani, H., Olmo, F. J., Andrey, J., and Alados-Arboledas, L.: Study of mineral dust entrainment in the planetary boundary layer by lidar depolarisation technique, Tellus B, 67, 26180, D14S04, doi:10.1029/2007JD009582, 2015.

Cachorro, V. E., Toledano, C., Prats, N., Sorribas, M., Mogo, S., Berjón, A., Torres, B., Rodrigo, R., De la Rosa, J., and De Frutos, A. M.: The strongest desert dust intrusion mixed with smoke over the Iberian Peninsula registered with Sun photometry, J. Geophys. Res.-Atmos., 113, D14S04, doi:10.1029/2007JD009582, 2008.

AMTD
8, 9289–9338, 2015

Chaikovsky, A., Dubovik, O., Goloub, P., Balashevich, N., Lopatsin, A., Karol, Y., Denisov, S., and Lapyonok, T.: Software package for the retrieval of aerosol microphysical properties in the vertical column using combined lidar/photometer data (test version), Tech. rep., Institute of Physics, National Academy of Sciences of Belarus, Minsk, Belarus, 2008.

Chaikovsky, A., Dubovik, O., Goloub, P., Tanre, D., Pappalardo, G., Wandinger, U., Chaikovskaya, L., Denisov, S., Grudo, Y., Lopatsin, A., Karol, Y., Lapyonok, T., Korol, M., Osipenko, F., Savitski, D., Slesar, A., Apituley, A., Arboledas, L. A., Binietoglou, I., Kokkalis, P., Granados Muñoz, M. J., Papayannis, A., Perrone, M. R., Pietruczuk, A., Pisani, G., Rocadenbosch, F., Sicard, M., De Tomasi, F., Wagner, J., and Wang, X.: Algorithm and software for the retrieval of vertical aerosol properties using combined lidar/radiometer data: dissemination in EARLINET, in: Proceedings of the 26 International Laser and Radar Conference, vol. 1, 25–29 June 2012, Porto Heli, Greece, 399–402, 2012.

Chen, Y. and Penner, J. E.: Uncertainty analysis for estimates of the first indirect aerosol effect, Atmos. Chem. Phys., 5, 2935–2948, doi:10.5194/acp-5-2935-2005, 2005.

Choobari, O. A., Zawar-Reza, P., and Sturman, A.: The global distribution of mineral dust and its impacts on the climate system: a review, Atmos. Res., 138, 152–165, 2014.

Córdoba-Jabonero, C., Sorribas, M., Guerrero-Rascado, J. L., Adame, J. A., Hernández, Y., Lyamani, H., Cachorro, V., Gil, M., Alados-Arboledas, L., Cuevas, E., and de la Morena, B.: Synergetic monitoring of Saharan dust plumes and potential impact on surface: a case study of dust transport from Canary Islands to Iberian Peninsula, Atmos. Chem. Phys., 11, 3067–3091, doi:10.5194/acp-11-3067-2011, 2011.

Creamean, J. M., Suski, K. J., Rosenfeld, D., Cazorla, A., DeMott, P. J., Sullivan, R. C., White, A. B., Ralph, F. M., Minnis, P., Comstock, J. M., Tomlinson, J. M., and Prather, K. A.: Dust and biological aerosols from the Sahara and Asia influence precipitation in the western US, Science, 339, 1572–1578, doi:10.1126/science.1227279, 2013.

DeMott, P. J. and Prenni, A. J.: New directions: need for defining the numbers and sources of biological aerosols acting as ice nuclei, Atmos. Environ., 44, 1944–1945, 2010.

Dubovik, O. and King, M. D.: A flexible inversion algorithm for retrieval of aerosol optical properties from sun and sky radiance measurements, J. Geophys. Res.-Atmos., 105, 20673–20696, 2000.

Dubovik, O., Smirnov, A., Holben, B. N., King, M. D., Kaufman, Y. J., Eck, T. F., and Slutsker, I.: Accuracy assessments of aerosol optical properties retrieved from aerosol robotic network

AMTD
8, 9289–9338, 2015

(AERONET) sun and sky radiance measurements, J. Geophys. Res.-Atmos., 105, 9791–9806, 2000.
Dubovik, O., Holben, B., Eck, T. F., Smirnov, A., Kaufman, Y. J., King, M. D., Tanré, D., and Slutsker, I.: Variability of absorption and optical properties of key aerosol types observed in worldwide locations, J. Atmos. Sci., 59, 590–608, 2002.
Dubovik, O., Sinyuk, A., Lapyonok, T., Holben, B. N., Mishchenko, M., Yang, P., Eck, T. F., Volten, H., Munoz, O., Weihelmann, B., van der Zande, W. J., Leon, J. F., Sokorin, M., and Slutsker, I.: Application of spheroid models to account for aerosol particle nonsphericity in remote sensing of desert dust, J. Geophys. Res.-Atmos., 111, D11208, doi:10.1029/2005JD006619, 2006.
Fairlie, T. D., Jacob, D. J., Dibb, J. E., Alexander, B., Avery, M. A., van Donkelaar, A., and Zhang, L.: Impact of mineral dust on nitrate, sulfate, and ozone in transpacific Asian pollution plumes, Atmos. Chem. Phys., 10, 3999–4012, doi:10.5194/acp-10-3999-2010, 2010.
Feingold, G., Furrer, R., Pilewskie, P., Remer, L. A., Min, Q., and Jonsson, H.: Aerosol indirect effect studies at Southern Great Plains during the May 2003 intensive operations period, J. Geophys. Res., 111, D05S14, doi:10.1029/2004JD005648, 2006.
Ferek, R. J., Garrett, T., Hobbs, P. V., Strader, S., Johnson, D., Taylor, J. P., Nielsen, K., Ackerman, A. S., Kogan, Y., and Liu, Q.: Drizzle suppression in ship tracks, J. Atmos. Sci., 57, 2707–2728, 2000.
Fernald, F. G.: Analysis of atmospheric lidar observations – some comments, Appl. Optics, 23, 652–653, 1984.
Fernald, F. G., Herman, B. M., and Reagan, J. A.: Determination of aerosol height distributions by lidar, J. Appl. Meteorol., 11, 482–489, 1972.
Formenti, P., Schütz, L., Balkanski, Y., Desboeufs, K., Ebert, M., Kandler, K., Petzold, A., Scheuvens, D., Weinbruch, S., and Zhang, D.: Recent progress in understanding physical and chemical properties of African and Asian mineral dust, Atmos. Chem. Phys., 11, 8231–8256, doi:10.5194/acp-11-8231-2011, 2011.
Ginoux, P.: Effects of nonsphericity on mineral dust modeling, J. Geophys. Res.-Atmos., 108, 4052, doi:10.1029/2002JD002516, 2003.
Glen, A. and Brooks, S. D.: A new method for measuring optical scattering properties of atmospherically relevant dusts using the cloud and aerosol spectrometer with polarization (CASPOL), Atmos. Chem. Phys., 13, 1345–1356, doi:10.5194/acp-13-1345-2013, 2013.

AMTD
8, 9289–9338, 2015

Granados-Muñoz, M. J., Guerrero-Rascado, J. L., Bravo-Aranda, J. A., Navas-Guzmán, F., Valenzuela, A., Lyamani, H, Chaikovsky, A., Wandinger, U., Ansmann, A., Dubovik, O., Grudo, J. O., and Alados-Arboledas, L.: Retrieving aerosol microphysical properties by lidar-radiometer inversion code (LIRIC) for different aerosol types, J. Geophys. Res.-Atmos., 119, 4836–4858, 2014.

Gross, S., Tesche, M., Freudenthaler, V., Toledano, C., Wiegner, M., Ansmann, A., Althausen, D., and Seefeldner, M.: Characterization of Saharan dust, marine aerosols and mixtures of biomass-burning aerosols and dust by means of multi-wavelength depolarization and raman lidar measurements during SAMUM 2, Tellus B, 63: 706–724, doi:10.1111/j.1600-0889.2011.00556.x, 2011.

Guerrero-Rascado, J. L., Ruiz, B., and Alados-Arboledas, L.: Multi-spectral lidar characterization of the vertical structure of Saharan dust aerosol over southern Spain, Atmos. Environ., 42, 2668–2681, 2008.

Guerrero-Rascado, J. L., Olmo, F. J., Avilés-Rodríguez, I., Navas-Guzmán, F., Pérez-Ramírez, D., Lyamani, H., and Alados Arboledas, L.: Extreme Saharan dust event over the southern Iberian Peninsula in september 2007: active and passive remote sensing from surface and satellite, Atmos. Chem. Phys., 9, 8453–8469, doi:10.5194/acp-9-8453-2009, 2009.

Gunn, R. and Phillips, B. B.: An experimental investigation of the effect of air pollution on the initiation of rain, J. Meterol., 14, 272–280, 1957.

Holben, B. N., Eck, T. F., Slutsker, I., Tanre, D., Buis, J. P., Setzer, A., Vermote, E., Reagan, J. A., Kaufman, Y. J., Nakajima, T., Lavenu, F., Jankowiak, I., and Smirnov, A.: AERONET – a Federated instrument network and data archive for aerosol characterization, Remote Sens. Environ., 66, 1–16, 1998.

Kazadzis, S., Veselovskii, I., Amiridis, V., Gröbner, J., Suvorina, A., Nyeki, S., Gerasopoulos, E., Kouremeti, N., Taylor, M., Tsekeri, A., and Wehrli, C.: Aerosol microphysical retrievals from precision filter radiometer direct solar radiation measurements and comparison with AERONET, Atmos. Meas. Tech., 7, 2013–2025, doi:10.5194/amt-7-2013-2014, 2014.

Klett, J. D.: Stable analytical inversion solution for processing lidar returns, Appl. Optics, 20, 211–220, 1981.

Klett, J. D.: Lidar inversion with variable backscatter/extinction ratios, Appl. Optics, 24, 1638–1643, 1985.

AMTD
8, 9289–9338, 2015

Levy, R. C., Mattoo, S., Munchak, L. A., Remer, L. A., Sayer, A. M., Patadia, F., and Hsu, N. C.: The Collection 6 MODIS aerosol products over land and ocean, Atmos. Meas. Tech., 6, 2989–3034, doi:10.5194/amt-6-2989-2013, 2013.

Liou, K. N. and Ou, S. C.: The role of cloud microphysical processes in climate: an assessment from a one-dimensional perspective, J. Geophys. Res.-Atmos., 94, 8599–8607, 1989.

Lopatin, A., Dubovik, O., Chaikovsky, A., Goloub, P., Lapyonok, T., Tanré, D., and Litvinov, P.: Enhancement of aerosol characterization using synergy of lidar and sun-photometer coincident observations: the GARRLiC algorithm, Atmos. Meas. Tech., 6, 2065–2088, doi:10.5194/amt-6-2065-2013, 2013.

Lyamani, H., Olmo, F. J., and Alados-Arboledas, L.: Saharan dust outbreak over south-eastern Spain as detected by sun-photometer, Atmos. Environ., 39, 7276–7284, doi:10.1016/j.atmosenv.2005.09.011, 2005.

Lyamani, H., Olmo, F. J., and Alados-Arboledas, L.: Light scattering and absorption properties of aerosol particles in the urban environment of Granada, Spain. Atmos. Environ., 42, 2630–2642, 2008.

Lyamani, H., Olmo, F. J., and Alados-Arboledas, L.: Physical and optical properties of aerosols over an urban location in Spain: seasonal and diurnal variability, Atmos. Chem. Phys., 10, 239–254, doi:10.5194/acp-10-239-2010, 2010.

Lyamani, H., Fernández-Gálvez, J., Pérez-Ramírez, D., Valenzuela, A., Antón, M., Alados, I., Titos, G., Olmo, F. J., and Alados-Arboledas, L.: Aerosol properties over two urban sites in South Spain during an extended stagnation episode in winter season, Atmos. Environ., 62, 424–432, 2012.

McConnell, C. L., Formenti, P., Highwood, E. J., and Harrison, M. A. J.: Using aircraft measurements to determine the refractive index of Saharan dust during the DODO Experiments, Atmos. Chem. Phys., 10, 3081–3098, doi:10.5194/acp-10-3081-2010, 2010.

McCormick, R. A. and Ludwig, J. H.: Climate modification by atmospheric aerosols, Science, 156, 1358–1359, 1967.

Miller, R. L. and Tegen, I.: Climate response to soil dust aerosols, J. Climate, 11, 3247–3267, 1998.

Mishchenko, M. I., Travis, L. D., Kahn, R. A., and West, R. A.: Modeling phase functions for dust like tropospheric aerosols using a shape mixture of randomly oriented polydisperse spheroids, J. Geophys. Res., 102, 16831–16848, 1997.

AMTD
8, 9289–9338, 2015

Mona, L., Amodeo, A., Pandolfi, M., and Pappalardo, G.: Saharan dust intrusions in the Mediterranean area: three years of raman lidar measurements, J. Geophys. Res.-Atmos., 111, D16203, doi:10.1029/2005JD006569, 2006.

Murayama, T., Masonis, S. J., Redemann, J., Anderson, T. L., Schmid, B., Livingston, J. M., Russell, P. B., Huebert, B., Howell, S. G., McNaughton, C. S., Clarke, A., Abo, M., Shimizu, A., Sugimoto, N., Yabuki, M., Kuze, H., Fukagawa, S., Maxwell-Meier, K., Weber, R. J., Orsini, D. A., Blomquist, B., Bandy, A., and Thornton, D.: An intercomparison of lidar-derived aerosol optical properties with airborne measurements near Tokyo during ACE-Asia, J. Geophys. Res., 108, 8651, doi:10.1029/2002JD003259, 2003.

Navas-Guzmán, F., Guerrero-Rascado, J. L., and Alados-Arboledas, L.: Retrieval of the lidar overlap function using raman signals, Opt. Pura Apl., 44, 71–75, 2011.

Navas-Guzmán, F., Bravo-Aranda, J. A., Guerrero-Rascado, J. L., Granados-Muñoz, M. J., and Alados-Arboledas, L.: Statistical analysis of aerosol optical properties retrieved by Raman lidar over Southeastern Spain, Tellus B, 65, 21234, doi:10.3402/tellusb.v65i0.21234, 2013.

Nicolet, M., Stetzer, O., and Lohmann, U. : Depolarization ratios of singles ice particles assuming finite circular cylinders, Appl. Optics, 46, 4465–4476, 2007.

Nicolet, M., Stetzer, O., Lüönd, F., Möhler, O., and Lohmann, U.: Single ice crystal measurements during nucleation experiments with the depolarization detector IODE, Atmos. Chem. Phys., 10, 313–325, doi:10.5194/acp-10-313-2010, 2010.

Nicolet, M., Schnaiter, M., and Stetzer, O.: Circular depolarization ratios of single water droplets and finite ice circular cylinders: a modeling study, Atmos. Chem. Phys., 12, 4207–4214, doi:10.5194/acp-12-4207-2012, 2012.

Olmo, F. J., Quirantes, A., Alcántara, A., Lyamani, H., and Alados-Arboledas, L.: Preliminary results of a non-spherical aerosol method for the retrieval of the atmospheric aerosol optical properties, J. Quant. Spectrosc. Ra., 100, 305–314, 2006.

O'Neill, N. T., Dubovik, O., and Eck, T. F.: Modified Ångström exponent for the characterization of submicrometer aerosols, Appl. Optics, 40, 2368–2375, 2001a.

O'Neill, N. T., Eck, T. F., Holben, B., Smirnov, A., and Dubovik, O.: Bimodal size distribution influences on the variation of Angstrom derivatives in spectral and optical depth space, J. Geophys. Res., 106, 9787–9806, 2001b.

O'Neill, N. T., Eck, T. F., Smirnov, A., Holben, B. N., and Thulasiraman, S.: Spectral discrimination of coarse and fine mode optical depth, J. Geophys. Res.-Atmos., 108, 4559, doi:10.1029/2002JD002975, 2003.

AMTD
8, 9289–9338, 2015

O'Neill, N. T., Eck, T. F., Reid, J. S., Smirnov, A., and Pancrati, O.: Coarse mode optical information retrievable using ultraviolet to short-wave infrared sun photometry: application to united arab emirates unified aerosol experiment data, J. Geophys. Res., 113, D05212, doi:10.1029/2007JD009052, 2008.

Papayannis, A., Balis, D., Amiridis, V., Chourdakis, G., Tsaknakis, G., Zerefos, C., Castanho, A. D. A., Nickovic, S., Kazadzis, S., and Grabowski, J.: Measurements of Saharan dust aerosols over the Eastern Mediterranean using elastic backscatter-Raman lidar, spectrophotometric and satellite observations in the frame of the EARLINET project, Atmos. Chem. Phys., 5, 2065–2079, doi:10.5194/acp-5-2065-2005, 2005.

Papayannis, A., Amiridis, V., Mona, L., Tsaknakis, G., Balis, D., Bösenberg, J., Chaikovski, A., De Tomasi, F., Grigorov, I., and Mattis, I.: Systematic lidar observations of Saharan dust over Europe in the frame of EARLINET (2000–2002), J. Geophys. Res.-Atmos., 113, D10204, doi:10.1029/2007JD009028, 2008.

Papayannis, A., Mamouri, R. E., Amiridis, V., Remoundaki, E., Tsaknakis, G., Kokkalis, P., Veselovskii, I., Kolgotin, A., Nenes, A., and Fountoukis, C.: Optical-microphysical properties of Saharan dust aerosols and composition relationship using a multi-wavelength Raman lidar, in-situ sensors and modelling: a case study analysis, Atmos. Chem. Phys., 12, 4011–4032, doi:10.5194/acp-12-4011-2012, 2012.

Pappalardo, G., Amodeo, A., Pandolfi, M., Wandinger, U., Ansmann, A., Bösenberg, J., Matthias, V., Amiridis, V., De Tomasi, F., and Frioud, M.: Aerosol lidar intercomparison in the framework of the EARLINET project, 3. raman lidar algorithm for aerosol extinction, backscatter, and lidar ratio, Appl. Optics, 43, 5370–5385, 2004.

Pappalardo, G., Papayannis, A., Bösenberg, J., Ansmann, A., Apituley, A., Alados-Arboledas, L., Balis, D., Böckmann, C., Chaikovsky, A., Comeron, A., Gustafsson, O., Hansen, G., Mitev, V., Mona, L., Nicolae, D., Perrone, M. R., Pietruczuk, A., Pujadas, M., Putaud, J. P., Ravetta, F., Rizi, V., Simeonov, V., Spinelli, N., Stoyanov, D., Trickl, T., and Wiegner, M.: EARLINET coordinated lidar observations of Saharan dust events on continental scale, in: IOP Conference Series: Earth and Environmental Science, WMO/GEO Expert Meeting on an International Sand and Dust Storm Warning System, Barcelona, Spain, 7–9 November 2007, Vol. 7, 012002, doi:10.1088/1755-1307/7/1/012002, 2009.

Pappalardo, G., Amodeo, A., Apituley, A., Comeron, A., Freudenthaler, V., Linné, H., Ansmann, A., Bösenberg, J., D'Amico, G., Mattis, I., Mona, L., Wandinger, U., Amiridis, V., Alados-Arboledas, L., Nicolae, D., and Wiegner, M.: EARLINET: towards an ad-

AMTD
8, 9289–9338, 2015

vanced sustainable European aerosol lidar network, Atmos. Meas. Tech., 7, 2389–2409, doi:10.5194/amt-7-2389-2014, 2014.
Perez-Ramirez, D., Aceituno, J., Ruiz, B., Olmo, F. J., and Alados-Arboledas, L.: Development and calibration of a star-photometer to measure the aerosol optical depth: smoke observations at a high mountain site, Atmos. Environ., 42, 2733–2738, 2008a.
Perez-Ramirez, D., Aceituno, J., Ruiz, B., Olmo, F. J., and Alados-Arboledas, L.: Application of sun/star photometry to derive the aerosol optical depth, Int. J. Remote Sens., 29, 5113–5132, 2008b.
Perez-Ramirez, D., Lyamani, H., Olmo, F. J., and Alados Arboledas, L.: Improvements in star photometry for aerosol characterizations, J. Aerosol Sci., 4, 737–745, 2011.
Pérez-Ramírez, D., Lyamani, H., Olmo, F. J., Whiteman, D. N., and Alados-Arboledas, L.: Columnar aerosol properties from sun-and-star photometry: statistical comparisons and day-to-night dynamic, Atmos. Chem. Phys., 12, 9719–9738, doi:10.5194/acp-12-9719-2012, 2012a.
Pérez-Ramírez, D., Lyamani, H., Olmo, F. J., Whiteman, D. N., Navas-Guzmán, F., and Alados-Arboledas, L.: Cloud screening and quality control algorithm for star photometer data: assessment with lidar measurements and with all-sky images, Atmos. Meas. Tech., 5, 1585–1599, doi:10.5194/amt-5-1585-2012, 2012b.
Pérez-Ramírez, D., Veselovskii, I., Whiteman, D. N., Suvorina, A., Korenskiy, M., Kolgotin, A., Holben, B., Dubovik, O., Siniuk, A., and Alados-Arboledas, L.: High temporal resolution estimates of columnar aerosol microphysical parameters from spectrum of aerosol optical depth by linear estimation: application to long-term AERONET and star-photometry measurements, Atmos. Meas. Tech., 8, 3117–3133, doi:10.5194/amt-8-3117-2015, 2015.
Preißler, J., Wagner, F., Guerrero-Rascado, J. L., and Silva, A. M.: Two years of free-tropospheric aerosol layers observed over Portugal by lidar, J. Geophys. Res.-Atmos., 118, 2169–8996, doi:10.1002/jgrd.50350, 2013.
Rodríguez, S., Alastuey, A., Alonso-Pérez, S., Querol, X., Cuevas, E., Abreu-Afonso, J., Viana, M., Pérez, N., Pandolfi, M., and de la Rosa, J.: Transport of desert dust mixed with North African industrial pollutants in the subtropical Saharan Air Layer, Atmos. Chem. Phys., 11, 6663–6685, doi:10.5194/acp-11-6663-2011, 2011.
Rosenfeld, D., Rudich, Y., and Lahav, R.: Desert dust suppressing precipitation: a possible desertification feedback loop, in: Proceedings of the National Academy of Sciences of the United States of America, 98, 5975–5980, doi:10.1073/pnas.101122798, 2001.

AMTD
8, 9289–9338, 2015

Sabatier, P. C.: Basic concepts and methods of inverse problems, in: Basic Methods of Tomography and Inverse Problems, Adam Hilger, Philadelphia, USA, 1987.

Schnaiter, M., Büttner, S., Möhler, O., Skrotzki, J., Vragel, M., and Wagner, R.: Influence of particle size and shape on the backscattering linear depolarisation ratio of small ice crystals – cloud chamber measurements in the context of contrail and cirrus microphysics, Atmos. Chem. Phys., 12, 10465–10484, doi:10.5194/acp-12-10465-2012, 2012.

Seifert, P., Ansmann, A., Mattis, I., Wandinger, U., Tesche, M., Engelmann, R., Müller, D., Pérez, C., and Haustein, K.: Saharan dust and heterogeneous ice formation: eleven years of cloud observations at a central European EARLINET site, J. Geophys. Res.-Atmos, 115, D20201, doi:10.1029/2009JD013222, 2010.

Shao, Y., Wyrwoll, K. H., Chappell, A., Huang, J., Lin, Z., McTainsh, G. H., Mikami, M., Tanaka, T., Wang, X., and Yoon, S.: Dust cycle: an emerging core theme in Earth system science, Aeolian Research, 2, 181–204, 2011.

Sokolik, I. N. and Toon, O. B.: Incorporation of mineralogical composition into models of the radiative properties of mineral aerosol from UV to IR wavelengths, J. Geophys. Res.-Atmos., 104, 9423–9444, 1999.

Tesche, M., Gross, S., Ansmann, A., Mueller, D., Althausen, D., Freudenthaler, V., and Esselborn, M.: Profiling of Saharan dust and biomass-burning smoke with multiwavelength polarization raman lidar at Cape Verde, Tellus B, 63, 649–676, 2011.

Textor, C., Schulz, M., Guibert, S., Kinne, S., Balkanski, Y., Bauer, S., Berntsen, T., Berglen, T., Boucher, O., Chin, M., Dentener, F., Diehl, T., Feichter, J., Fillmore, D., Ginoux, P., Gong, S., Grini, A., Hendricks, J., Horowitz, L., Huang, P., Isaksen, I. S. A., Iversen, T., Kloster, S., Koch, D., Kirkevåg, A., Kristjansson, J. E., Krol, M., Lauer, A., Lamarque, J. F., Liu, X., Montanaro, V., Myhre, G., Penner, J. E., Pitari, G., Reddy, M. S., Seland, Ø., Stier, P., Takemura, T., and Tie, X.: The effect of harmonized emissions on aerosol properties in global models – an AeroCom experiment, Atmos. Chem. Phys., 7, 4489–4501, doi:10.5194/acp-7-4489-2007, 2007.

Tikhonov, A. N. and Arsenin, V. Y.: Methods for Solving Ill-Posed Problems, V. H. Winston & Sons, Washington, D.C., USA, 1977.

Titos, G., Foyo-Moreno, I., Lyamani, H., Querol, X., Alastuey, A., and Alados-Arboledas, L.: Optical properties and chemical composition of aerosol particles at an urban location: an estimation of the aerosol mass scattering and absorption efficiencies, J. Geophys. Res.-Atmos., 117, D04206, doi:10.1029/2011JD016671, 2012.

AMTD
8, 9289–9338, 2015

Titos, G., Lyamani, H., Pandolfi, M., Alastuey, A., and Alados-Arboledas, L.: Identification of fine (PM_1) and coarse (PM_{10-1}) sources of particulate matter in an urban environment, Atmos. Environ., 89, 593–602, 2014.

Tsekeri, A., Amiridis, V., Kokkalis, P., Basart, S., Chaikovsky, A., Dubovik, O., Papayannis, R., Baldasano, J. M., and Gross, B.: Application of a synergetic lidar and sunphotometer algorithm for the characterization of a dust event over Athens, Greece, British J. Environ. Clim. Change, 3, 531–546, 2013.

Twohy, C. H., Kreidenweis, S. M., Eidhammer, T., Browell, E. V., Heymsfield, A. J., Bansemer, A. R., Anderson, B. E., Chen, G., Ismail, S., and DeMott, P. J.: Saharan dust particles nucleate droplets in eastern Atlantic clouds, Geophys. Res. Lett., 36, L01807, doi:10.1029/2008GL035846, 2009.

Valenzuela, A., Olmo, F. J., Lyamani, H., Antón, M., Quirantes, A., and Alados-Arboledas, L.: Aerosol radiative forcing during African desert dust events (2005–2010) over Southeastern Spain, Atmos. Chem. Phys., 12, 10331–10351, doi:10.5194/acp-12-10331-2012, 2012a.

Valenzuela, A., Olmo, F. J., Lyamani, H., Antón, M., Quirantes, A., and Alados-Arboledas, L.: Analysis of the columnar radiative properties retrieved during African desert dust events over Granada (2005–2010) using principal plane sky radiances and spheroids retrieval procedure, Atmos. Res., 104, 292–301, 2012b.

Valenzuela, A., Olmo, F. J., Lyamani, H., Antón, M., Quirantes, A., and Alados-Arboledas, L.: Classification of aerosol radiative properties during African desert dust intrusions over southeastern Spain by sector origins and cluster analysis, J. Geophys. Res-Atmos., 117, D06214, doi:10.1029/2011JD016885, 2012c.

Veselovskii, I., Kolgotin, A., Griaznov, V., Müller, D., Wandinger, U., and Whiteman, D. N.: Inversion with regularization for the retrieval of tropospheric aerosol parameters from multiwavelength lidar sounding, Appl. Optics, 41, 3685–3699, 2002.

Veselovskii, I., Kolgotin, A., Griaznov, V., Müller, D., Franke, K., and Whiteman, D. N.: Inversion of multiwavelength raman lidar data for retrieval of bimodal aerosol size distribution, Appl. Optics, 43, 1180–1195, 2004.

Veselovskii, I., Dubovik, O., Kolgotin, A., Lapyonok, T., Di Girolamo, P., Summa, D., Whiteman, D. N., Mischenko, M., and Tanre, D.: Application of randomly oriented spheroids for retrieval of dust particle parameters from multiwavelength lidar measurements, J. Geophys. Res., 115, D21203, doi:10.1029/2010JD014139, 2010.

AMTD
8, 9289–9338, 2015

Veselovskii, I., Dubovik, O., Kolgotin, A., Korenskiy, M., Whiteman, D. N., Allakhverdiev, K., and Huseyinoglu, F.: Linear estimation of particle bulk parameters from multi-wavelength lidar measurements, Atmos. Meas. Tech., 5, 1135–1145, doi:10.5194/amt-5-1135-2012, 2012.
Veselovskii, I., Whiteman, D. N., Korenskiy, M., Kolgotin, A., Dubovik, O., Perez-Ramirez, D., and Suvorina, A.: Retrieval of spatio-temporal distributions of particle parameters from multiwavelength lidar measurements using the linear estimation technique and comparison with AERONET, Atmos. Meas. Tech., 6, 2671–2682, doi:10.5194/amt-6-2671-2013, 2013.
Volckens, J. and Peters, T. M.: Counting and particle transmission efficiency of the aerodynamic particle sizer, J. Aerosol Sci., 36, 1400–1408, 2005.
Wagner, F., Bortoli, D., Pereira, S. Costa, M. J., Silva, A. N. A., Weinzierl, B., Esselborn, M., Petzold, A., Rasp, K., and Heinold, B.: Properties of dust aerosol particles transported to Portugal from the Sahara desert, Tellus B, 61, 297–306, 2009.
Wagner, J., Ansmann, A., Wandinger, U., Seifert, P., Schwarz, A., Tesche, M., Chaikovsky, A., and Dubovik, O.: Evaluation of the Lidar/Radiometer Inversion Code (LIRIC) to determine microphysical properties of volcanic and desert dust, Atmos. Meas. Tech., 6, 1707–1724, doi:10.5194/amt-6-1707-2013, 2013.
Wandinger, U. and Ansmann, A.: Experimental determination of the lidar overlap profile with raman lidar, Appl. Optics, 41, 511–514, 2002.
Weinzierl, B., Petzold, A., Esselborn, M., Wirth, M., Rasp, K., Kandler, K., Schutz, L., Kopke, P., and Fiebig, M.: Airborne measurements of dust layer properties, particle size distribution and mixing state of Saharan dust during SAMUM 2006, Tellus, B61, 96–117, doi:10.1111/j.1600-0889.2008.00392.x, 2009.
Weinzierl, B., Sauer, D., Esselborn, M., Petzold, A., Veira, A., Rose, M., Mund, S., Wirth, M., Ansmann, A., Tesche, M., Gross, S., and Freudenthaler, V.: Microphysical and optical properties of dust and tropical biomass burning aerosol layers in the Cape Verde region – an overview of the airborne in-situ and lidar measurements during SAMUM-2, Tellus, B63, 589–618, doi:10.1111/j.1600-0889.2011.00566.x, 2011.
Zender, C. S., Bian, H., and Newman, D.: Mineral dust entrainment and deposition (DEAD) model: description and 1990s dust climatology, J. Geophys. Res., 108, 4416, doi:10.1029/2002JD002775, 2003.
Zender, C. S., Miller, R., and Tegen, I.: Quantifying mineral dust mass budgets: terminology, constraints, and current estimates, EOS T Am. Geophys. Un., 85, 509–512, 2004.

AMTD
8, 9289–9338, 2015

Table 1. Aerosol properties on region 1, corresponding to the mixture of anthropogenic aerosol and mineral dust below 2250 m a.s.l. and region 2, corresponding to the mineral dust particles located above 2250 m a.s.l.

	$\beta^{aer}_{532\,nm}$ ($Mm^{-1}\,sr^{-1}$)	$\delta^{P}_{532\,nm}$	β-AE (355–532 nm)	r_{eff} (μm)	V ($\mu m^3\,cm^{-3}$)
Region 1	38	0.15	0.18	0.61	44
Region 2	82	0.25	0.05	1.23	54

AMTD
8, 9289–9338, 2015

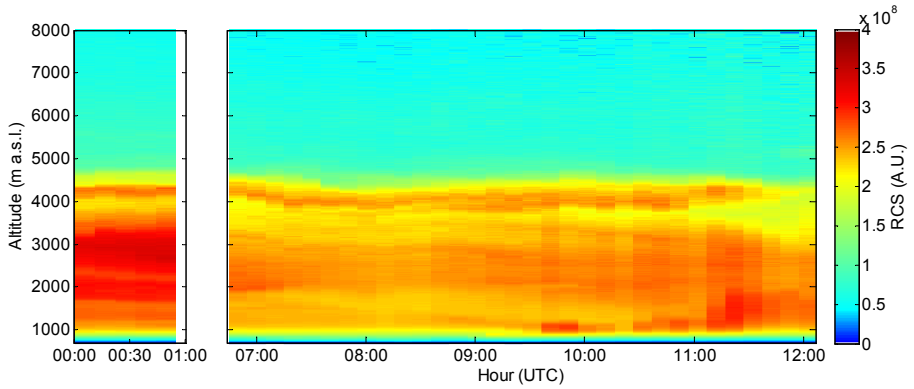

Figure 1. Time series of the RCS for the period 00:00–01:00 UTC and 06:45–12:10 UTC on the 27 June 2011.

AMTD
8, 9289–9338, 2015

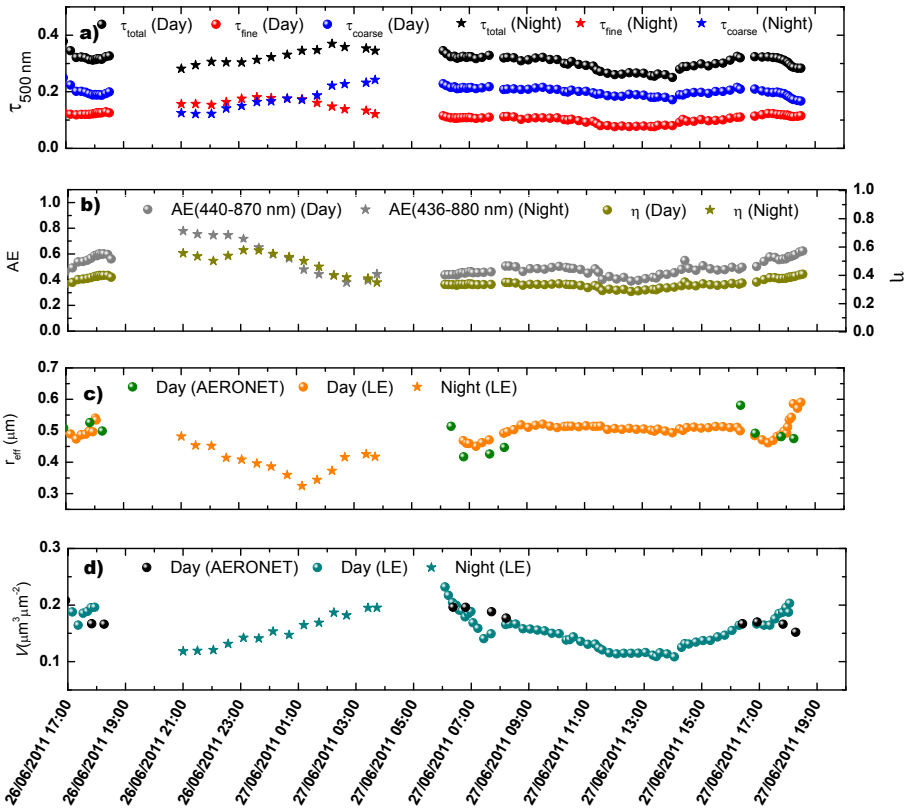

Figure 2. Night-to-day temporal evolution of **(a)** aerosol optical depth (τ_λ) including also its separation between fine (τ_{fine}) and coarse (τ_{coarse}) mode at 500 nm, **(b)** Ångström exponent (AE) between 440 and 870 nm (436–880 nm for star photometry) and fine mode fraction η **(c)** effective radius (r_{eff}) and **(d)** column integrated volume concentration (V) on the 27 June 2011.

AMTD
8, 9289–9338, 2015

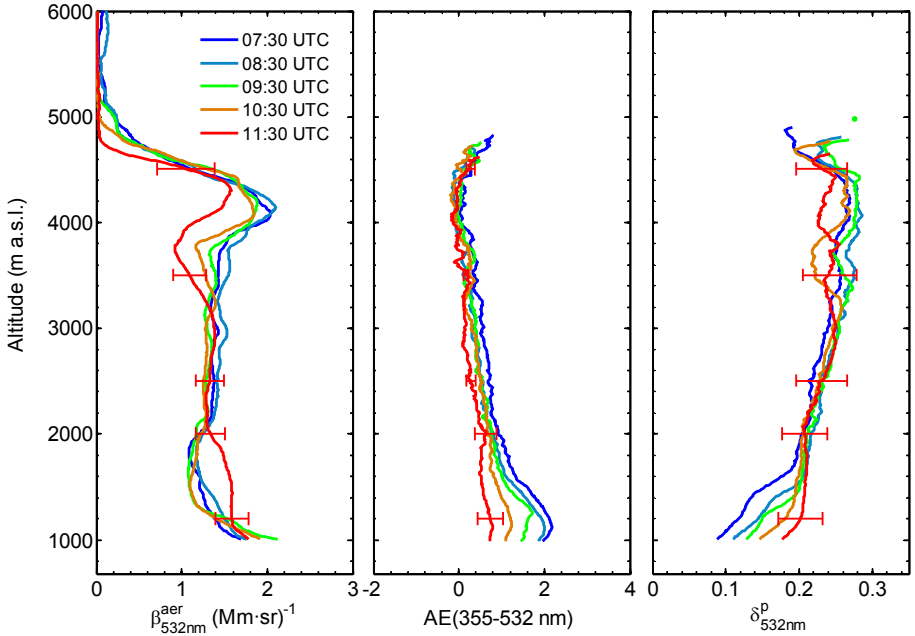

Figure 3. Profiles of **(a)** aerosol particle backscatter at 532 nm ($\beta^{\text{aer}}_{532\,\text{nm}}$) **(b)** backscatter-related Ångström exponent between 355 and 532 nm (β-AE(355–532 nm)) and **(c)** linear particle depolarization ratio at 532 nm ($\delta^{\text{P}}_{532\,\text{nm}}$) retrieved from lidar elastic measurements at different hours between 07:30 and 11:30 UTC on the morning of the 27 June 2011.

AMTD
8, 9289–9338, 2015

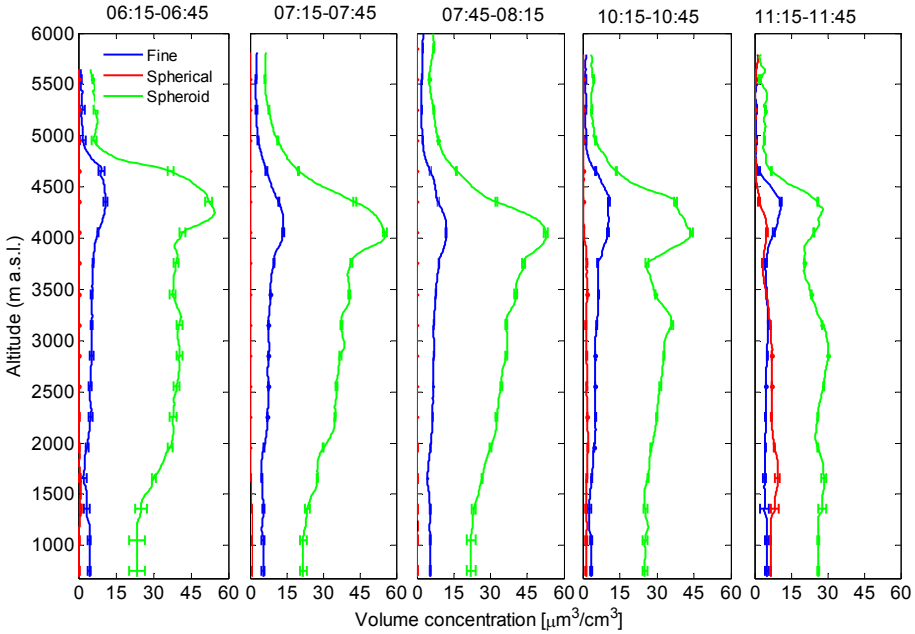

Figure 4. Volume concentration profiles of the fine, coarse spherical and coarse spheroid modes obtained with LIRIC from 30 min averaged lidar data for different periods on the 27 June 2011. The error bars are obtained as indicated in Granados-Muñoz et al. (2014).

AMTD
8, 9289–9338, 2015

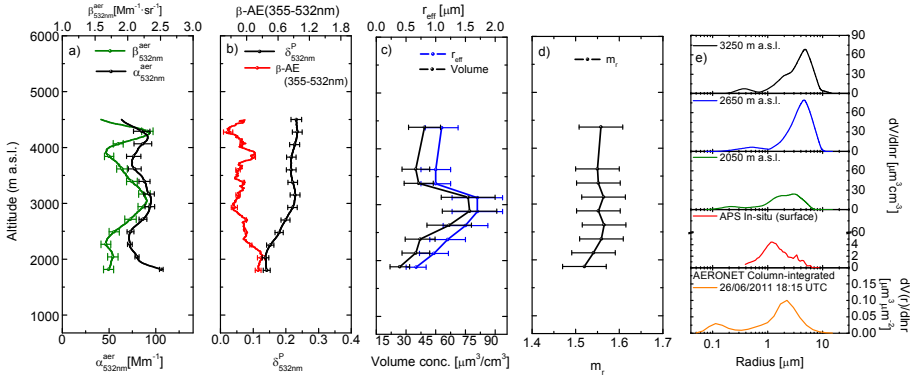

Figure 5. (a) $\beta^{aer}_{532\,nm}$ and $\alpha^{aer}_{532\,nm}$ retrieved with Raman technique and **(b)** derived β-AE(355–532 nm) and $\delta^{P}_{532\,nm}$ at 00:00–01:00 UTC on the 27 June 2011. **(c)** Total volume concentration, r_{eff} and **(d)** m_r retrieved for the same period with the regularization technique applied to the $3\beta + 2\alpha + 1\delta$ lidar data and **(e)** Volume size distributions retrieved at different height levels using the APS (surface level) and the regularization technique applied to the $3\beta + 2\alpha + 1\delta$ lidar data at 00:00–01:00 UTC on the 27 June 2011. Column-integrated AERONET size distribution corresponding to the 26 June 2011 at 18:15 UTC is included (bottom).

AMTD
8, 9289–9338, 2015

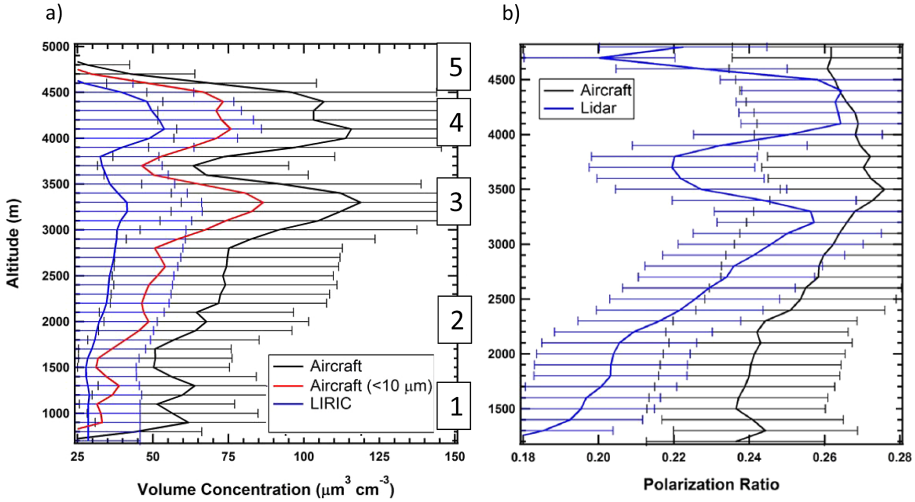

Figure 6. (a) 30 min averaged volume concentrations retrieved with LIRIC (blue line) centered at 10:30 UTC and the combined PCASP-100X and CAS-POL concentrations for particles smaller than 10 μm radius (red line) and for the complete size distritubion (black line) retrieved during the flight ascent on the 27 June 2011. **(b)** Depolarization ratio retrieved from the CAS-POL measurements (black line) and δP 532 nm retrieved from the lidar data (blue line) between 10:30 and 11:00 UTC. Horizontal bars show the estimated uncertainties.

AMTD
8, 9289–9338, 2015

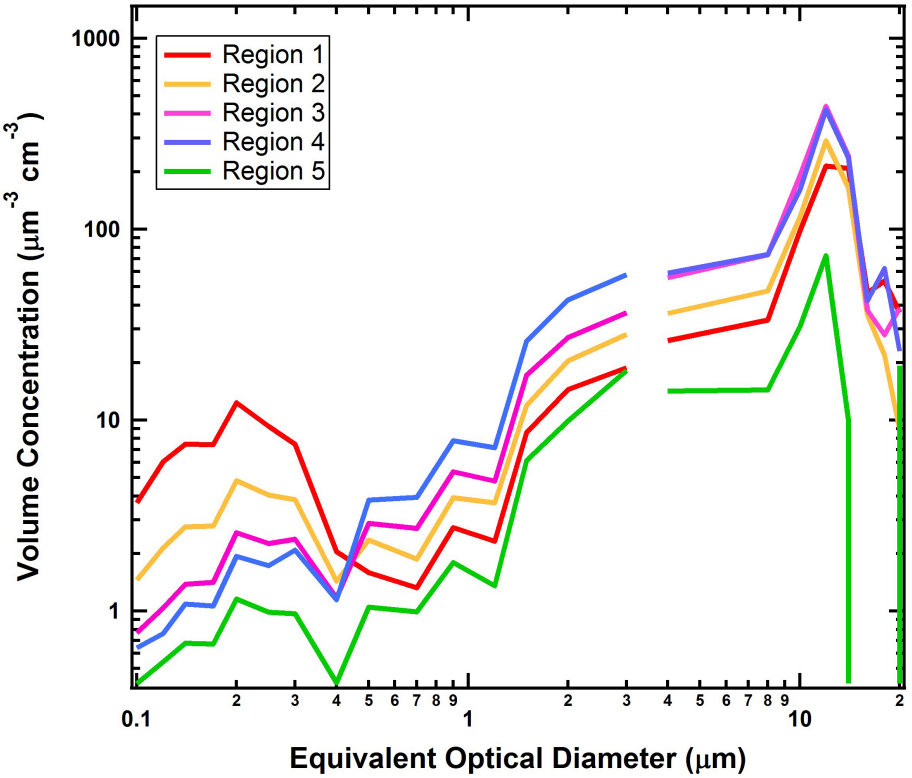

Figure 7. Size distributions of volume concentrations derived from the combined PCAP-100X and CAS-POL measurements averaged over the five altitude ranges labeled in Fig. 6a.

AMTD
8, 9289–9338, 2015

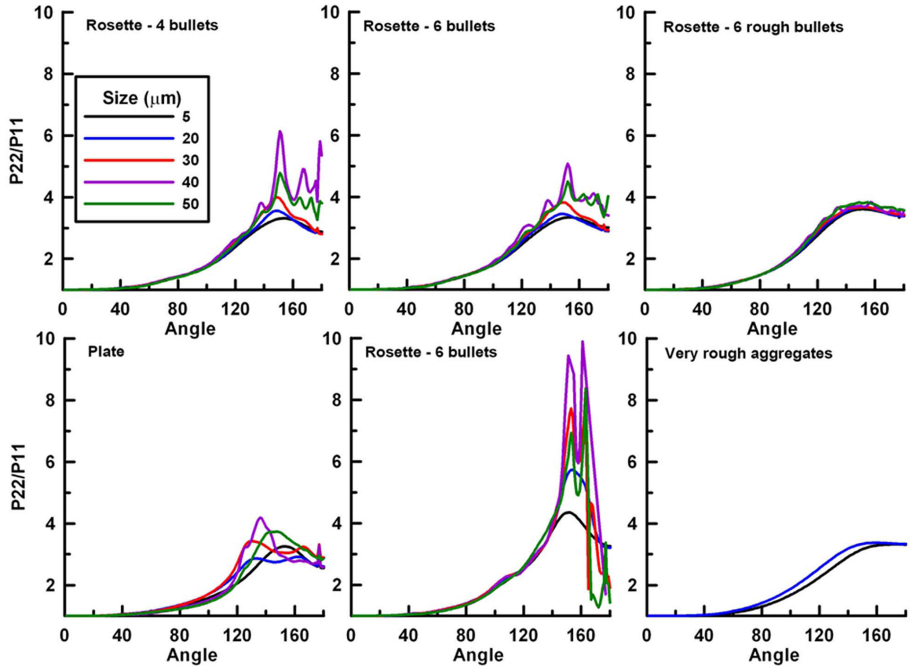

Figure 8. Theoretical calculations of the light scattering at 680 nm from individual ice crystals of different shapes and sizes (expressed in diameter) showing the ratio of the P_{22} and P_{11} components of the Stokes scattering matrix (calculations courtesy of Ping Yang, Texas A&M University).

AMTD
8, 9289–9338, 2015

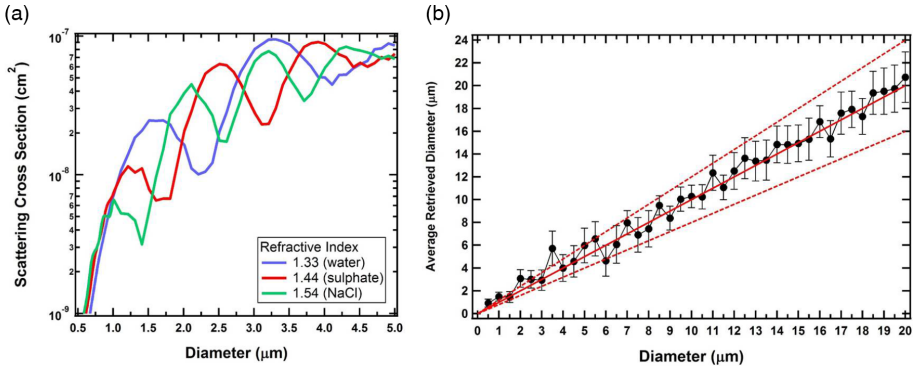

Figure 9. (a) Theoretical scattering cross section (Mie, 1908) of spherical particles as a function of diameter for three refractive indices and the collection angles of the CAS-POL. Only a small size range is shown in order to illustrate the potential magnitude of uncertainty. The dashed lines show that particles with four different sizes have the same scattering cross section. **(b)** Average retrieved diameter for a given size at a refractive index of 1.48. Vertical bars represent one standard deviation around the mean. The red lines are the one-to-one (solid) and ±20 % (dashed) around the one to one.

AMTD
8, 9289–9338, 2015

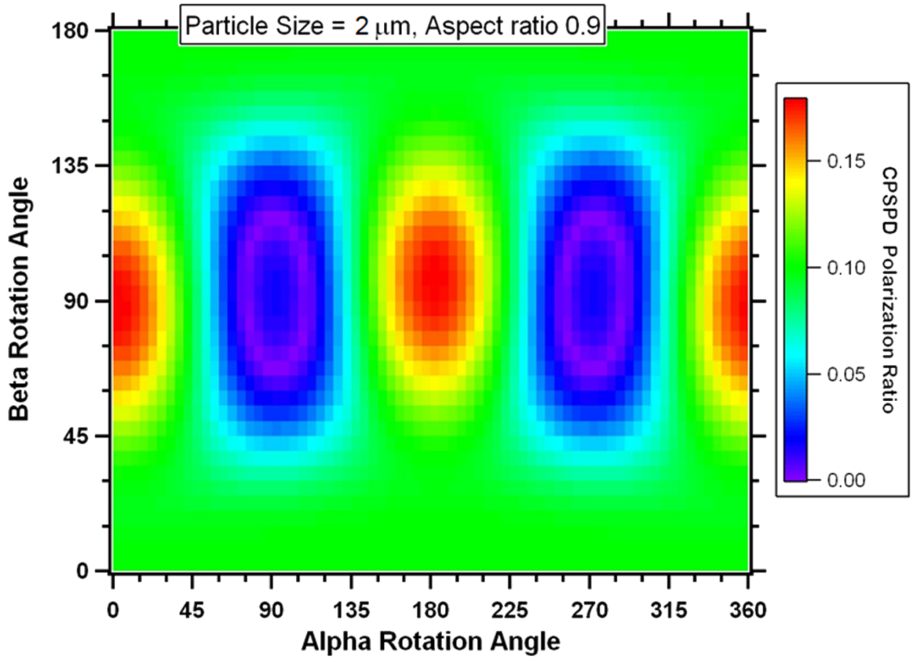

Figure 10. Response of the CAS-POL to a 2 µm particle with aspect ratio of 0.9 as a function of its orientation in the beam (alpha and beta represent the angles with respect to the incident laser beam).

AMTD
8, 9289–9338, 2015